Origin of $\delta 13C$ minimum events in thermocline and intermediate waters of the western South Atlantic

R.A. Nascimento, T.P. Santos, I.M. Venancio, C.M. Chiessi, J.M. Ballalai, H. Kuhnert, A. Govin, R.C. Portilho-Ramos, D. Lessa, B.B. Dias, et al.

HAL Id: hal-03434456
https://hal.science/hal-03434456

Submitted on 25 Nov 2021

1   **Origin of δ¹³C minimum events in thermocline and intermediate waters of the western**

2   **South Atlantic**

3   Nascimento, R. A[1*]; Santos, T. P.[1]; Venancio, I. M.[1,2]; Chiessi, C. M.[3]; Ballalai, J. M.[1]; Kuhnert,

4   H.[4]; Govin, A.[5]; Portilho-Ramos, R. C.[4]; Lessa, D.[1]; Dias, B. B.[1,3]; Pinho, T. M. L.[6]; Crivellari,

5   S.[3]; Mulitza, S.[4]; Albuquerque, A. L. S.[1]

6   [1] Programa de Geociências (Geoquímica), Universidade Federal Fluminense, Niterói, Brazil

7   [2] Center for Weather Forecasting and Climate Studies (CPTEC), National Institute for Space Research (INPE), Cachoeira Pau-

8   lista, Brazil

9   [3] School of Arts, Sciences and Humanities, University of São Paulo, São Paulo, Brazil

10   [4] MARUM - Center for Marine Environmental Sciences, University of Bremen, Bremen, Germany

11   [5] Laboratoire des Sciences du Climat et de l'Environnement/Institut Pierre Simon Laplace, CEA-CNRS-UVSQ, Université Paris

12   Saclay, Gif sur Yvette, France

13   [6] Institute of Geosciences, University of São Paulo, São Paulo, Brazil

14   *Corresponding author
15   e-mail address: rodrigoan@id.uff.br

17   **Abstract**

18   Stable carbon isotopic (δ¹³C) minimum events have been widely described in marine

19   archives recording the properties of thermocline and intermediate waters during glacial termi-

20   nations. However, the mechanisms associated with these events remain ambiguous. Here we

21   present three high temporal resolution deep-dwelling planktonic foraminifera δ¹³C records

22   from the main thermocline and one benthic δ¹³C record from the modern core of Antarctic

23   Intermediate Water (AAIW). Our sediment cores are distributed along the western South At-

24   lantic from the equator to the subtropics, with the longest record spanning the last ~300 kyr.

25   The results show that δ¹³C minimum events were pervasive features of the last three glacial

26   terminations and Marine Isotope Stage 4/3 transition in the western South Atlantic. Two dis-

27   tinct mechanisms were responsible for the δ¹³C minima at the thermocline and intermediate

28   depths of the Atlantic, respectively. We suggest that the δ¹³C minimum events at the thermo-

29   cline were mostly driven by the thermodynamic ocean-atmosphere isotopic equilibration,

30   which is supported by calculated δ¹³C of dissolved inorganic carbon in the subtropical western

31 South Atlantic as well as by previously published model simulations. On the other hand, inter-

32 mediate depths $\delta^{13}C$ minimum events in the tropics were likely caused by the slowdown of the

33 Atlantic meridional overturning circulation and the associated accumulation of isotopically light

34 carbon at mid and intermediate depths of the Atlantic Ocean.

35 **1. Introduction**

36   Upwelling in the Southern Ocean (SO) connects the deep ocean with the atmosphere,

37 by drawing deep waters to the SO surface (Marshall and Speer, 2012). The deep ocean is

38 hypothesized to have been the main sink of atmospheric CO_2 during glacial periods, as evi-

39 denced by the accumulation of ^{13}C-depleted remineralized carbon in poorly ventilated deep

40 waters below ~2500 m water depth (Hodell et al., 2003; Howe et al., 2016a; Curry and Oppo,

41 2005). Across glacial terminations, the breakup of deep-ocean stratification (e.g., Du et al.,

42 2018; Basak et al., 2018) and the intensification of upwelling in the SO have been linked to

43 the advection of nutrient-rich ^{13}C-depleted waters from the deep ocean to the SO surface (An-

44 derson et al., 2009; Toggweiler et al., 2006). This was followed by atmospheric CO_2 increase

45 and stable carbon isotopic ($\delta^{13}C$) minimum events at thermocline and intermediate depths of

46 the oceans (between 100 and 1200 m water depth) (e.g., Martínez-Botí et al., 2015; Ziegler et

47 al., 2013; Schmitt et al., 2012; Spero and Lea, 2002). A widely held hypothesis behind these

48 $\delta^{13}C$ minimum events is the northward transport of ^{13}C-depleted carbon from the SO surface

49 towards the equatorial regions by Subantarctic Mode Water (SAMW) and Antarctic Intermedi-

50 ate Water (AAIW) (Spero and Lea, 2002). This mechanism is named the "oceanic tunnel" (Liu

51 and Yang, 2003). In the Atlantic Ocean, the "oceanic tunnel" hypothesis is supported by the

52 occurrence of $\delta^{13}C$ minimum events in thermocline and intermediate depth records from the

53 tropical region (e.g., Poggemann et al., 2017; Mulitza et al., 1998). However, $\delta^{13}C$ minimum

54 events have also been observed in regions far from the influence of SAMW and AAIW as, for

55 example, in the North Atlantic (e.g., Lynch-Stieglitz et al., 2019; Rickaby and Elderfield, 2005).

56 Additionally, intermediate depth records in subtropical latitudes of the Southern Hemisphere

57   lack evidence of $\delta^{13}C$ minimum events. For instance, depth transects along the southern Bra-

58   zilian margin (~27°S) do not support the presence of a ^{13}C-depleted northward flowing AAIW

59   during Termination I (Lund et al., 2015; Tessin and Lund, 2013; Oppo and Horowitz, 2000).

60   Accordingly, other mechanisms have been raised to explain the occurrence of the $\delta^{13}C$ mini-

61   mum events.

62   The outgassing of ^{13}C-depleted CO_2 to the atmosphere during glacial terminations re-

63   sulted in an atmospheric ^{13}C depletion similar to that observed in the upper ocean (Eggleston

64   et al., 2016; Schmitt et al., 2012). Consequently, it has been suggested that temperature-

65   mediated ocean-atmosphere isotopic equilibration could explain the widespread occurrence

66   of $\delta^{13}C$ minimum events in the ocean (Shao et al., 2021; Lynch-Stieglitz et al., 2019; Ninne-

67   mann and Charles, 1997). According to this mechanism, the ocean-atmosphere isotopic equi-

68   libration would globally imprint the $\delta^{13}C$ minimum signal in the upper ocean and possibly at

69   intermediate and mid-depth waters at the formation region of these water masses.

70   Alternatively, $\delta^{13}C$ minima at intermediate depths of the tropical Atlantic may also have

71   been caused by changes in the dynamics of the Atlantic meridional overturning circulation

72   (AMOC) during glacial terminations, as indicated by model simulations (Menviel et al., 2018;

73   Schmittner and Lund, 2015). Some studies have suggested that the reduced ventilation rate

74   of North Atlantic Deep Water (NADW), which forms the lower limb of the AMOC, caused the

75   observed ^{13}C depletion in the mid-depth of the Atlantic Ocean during the last glacial termina-

76   tion (Campos et al., 2020; Lacerra et al., 2017; Schmittner and Lund, 2015; Lund et al., 2015).

77   Accordingly, this northern sourced ^{13}C-depletion may have expanded upwards into intermedi-

78   ate depths (~1000 m water depth) in the tropical Atlantic (Voigt et al., 2017; Freeman et al.,

79   2015). Ultimately, this could imply a northern origin for the $\delta^{13}C$ minimum signal at intermediate

80   depths of tropical regions.

81   Here we investigate the occurrence and origin of the $\delta^{13}C$ minimum events at the ther-

82   mocline and intermediate depths of the western South Atlantic during the last three glacial

83   terminations. We present three new high-resolution planktonic foraminiferal $\delta^{13}C$ records from

84   South Atlantic Central Water (SACW) and one record from AAIW extending from the equator

85   to the southern subtropical latitudes along the Brazilian margin (Fig. 1). Our results point to

86   two distinct and independent mechanisms governing the δ13C minimum events at the thermo-

87   cline and intermediate depths. At the thermocline, 13C-depletions were mostly driven by the

88   ocean-atmosphere isotopic equilibration, while AMOC slowdown was mostly responsible for

89   the 13C-depletion at intermediate depths.

2. Regional settings

91   The South Atlantic upper-ocean circulation is dominated by the South Atlantic Sub-

92   tropical Gyre (SASG) (Fig. 1a). The northernmost and the southernmost limits of the SASG

93   are marked by the South Equatorial Current (SEC) and the South Atlantic Current (SAC),

94   respectively. The westward-flowing SEC gives rise to the southward-flowing Brazil Current

95   (BC) and the northward-flowing North Brazil Undercurrent and North Brazil Current. At about

96   38°S, the BC converges with the northward-flowing Malvinas Current, giving rise to the SAC

97   that flows eastwards. Ultimately, the SAC feeds the SEC, which returns to the Brazilian coast,

98   closing the gyre (Peterson and Stramma, 1991).

99   The water masses filling thermocline and intermediate depths of the western South

100 Atlantic are SACW and AAIW (Fig. 1b), together named Southern Ocean intermediate waters

101 (SOIWs). The SACW occupies the South Atlantic thermocline between approximately 100 to

102 500 m water depth. This water mass shows wide temperature (5°C to 20°C) and salinity (34.3

103 to 36) ranges (Stramma and England, 1999). A portion of SACW is formed in the Brazil-Mal-

104 vinas Confluence zone (BMC) region at the subtropical convergence (Sprintall and Tomczak,

105 1993). During austral winter, the thick and homogeneous SAMW subducts in the subtropical

106 convergence, producing SACW, which moves eastward within the SAC and recirculates in the

107 SASG (Stramma and England, 1999). In the southeast Atlantic, another portion of SACW is

108 formed by the injection of Indian Ocean waters into the South Atlantic in the Agulhas Current

109 retroflection region (Poole and Tomczak, 1999; Sprintall and Tomczak, 1993; Gordon, 1986).

110 Below the SACW, AAIW is marked by minimum salinity between approximately 500 to 1500

111 m water depth (Fig. 1b). The temperature and salinity of the AAIW range between 2°C to 6°C

4

112   and 33.8 to 34.8, respectively (Emery and Meincke, 1986). AAIW is mainly formed by over-

113   turning convection in the extreme east of the South Pacific Ocean, enters the southwestern

114   Atlantic through the Drake Passage, and is carried northward in the Malvinas Current (England

115   et al. 1993). Northeast of the Drake Passage and at the BMC, mixing and eddy formation inject

116   AAIW into the South Atlantic subsurface (Stramma and England 1999; Talley, 1996). Addi-

117   tionally, substantial amounts of AAIW enter the Atlantic from the Indian Ocean through Agul-

118   has Current leakage around the southern tip of Africa (Stramma and England, 1999).

119   Below AAIW, the NADW fills the mid-depth of the Atlantic Ocean between ~1500 and

120   4000 m water depth. In the modern ocean, the core of NADW is centered at 2400 m water

121   depth (Fig. 1b). However, during the Last Glacial Maximum (LGM), NADW is estimated to

122   have shallowed to ~1800 m water depth (Gebbie, 2014). This water mass is formed in high

123   latitudes of the North Atlantic through buoyancy loss and convection of dense upper ocean

124   waters in the Labrador and Nordic Seas. NADW is featured by a salinity maximum (above

125   34.9) at mid-depth of the Atlantic Ocean (Fig. 1b) and a temperature ranging between 2 and

126   4°C (Tomczak and Godfrey, 1994).
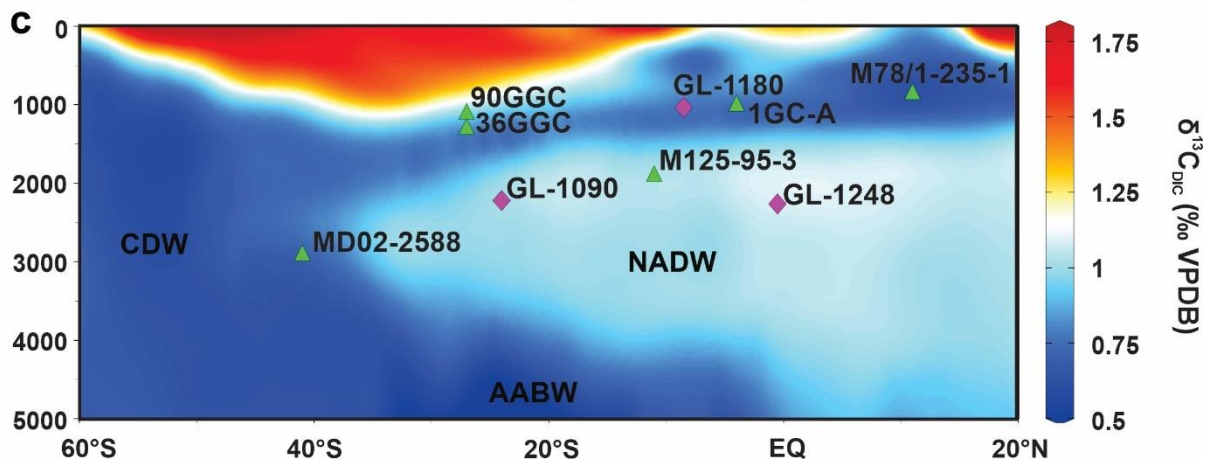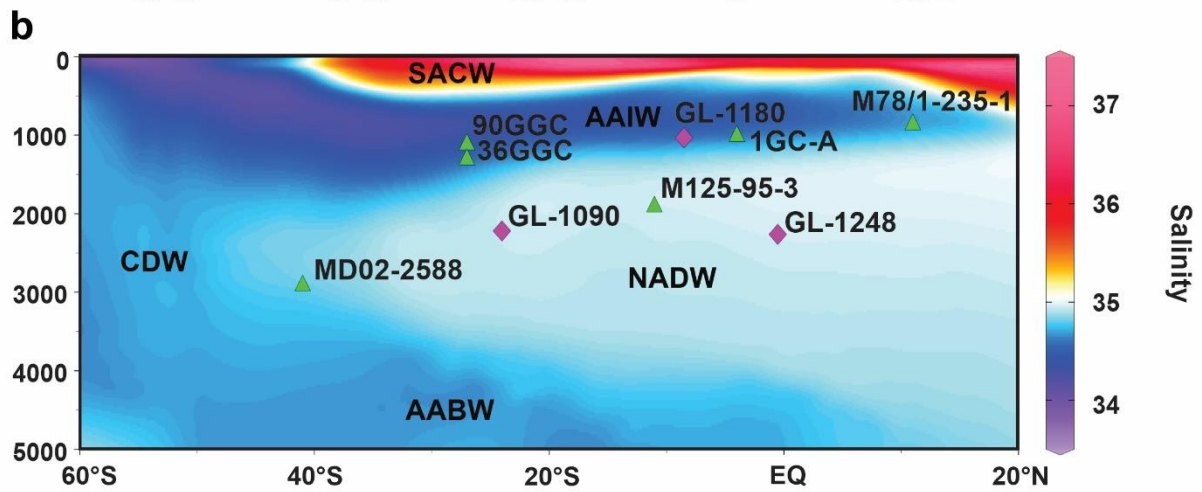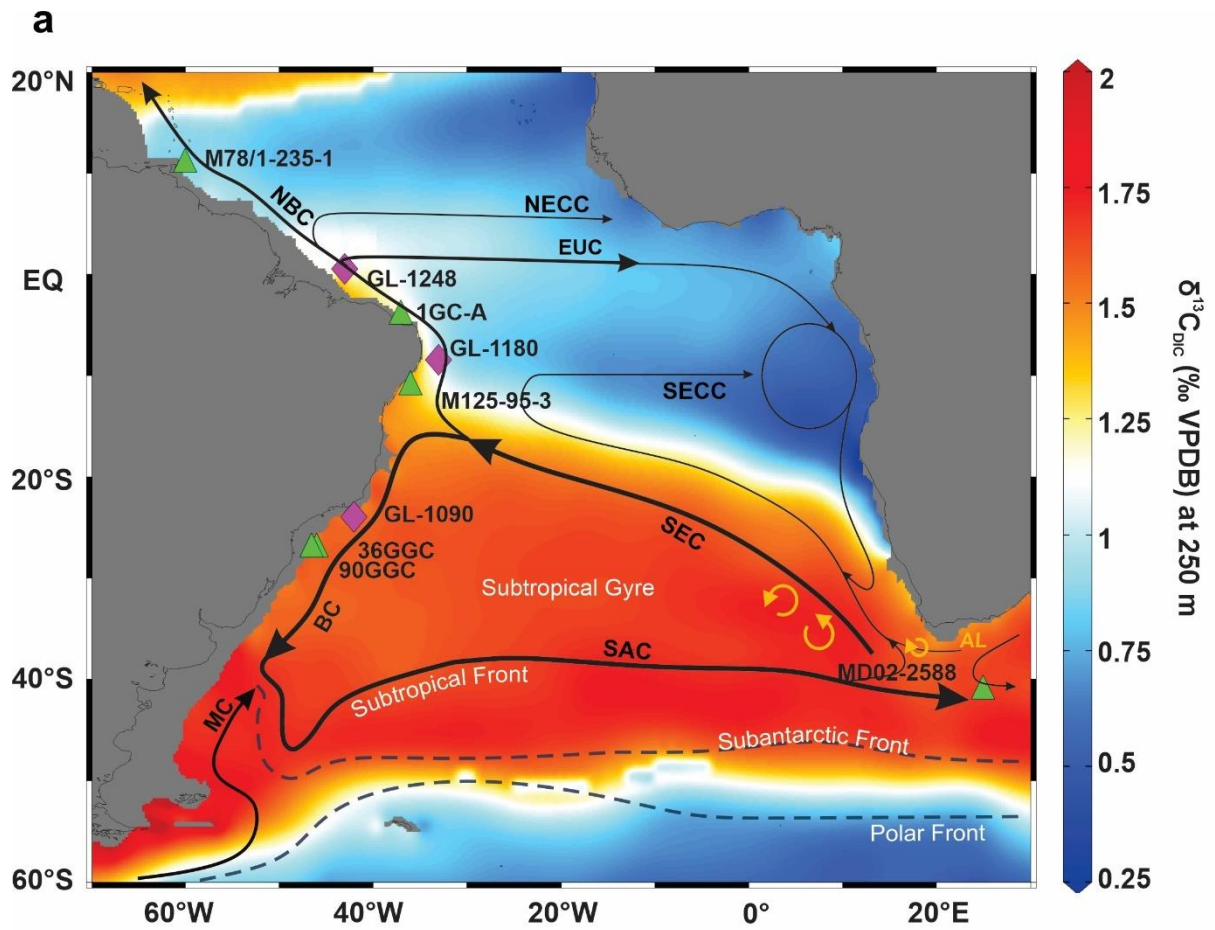
128   **Figure 1.** Location of the sediment cores analyzed in this study (pink diamonds) and other

129   sediment cores discussed within the text (green triangles). a) Atlantic Ocean pre-industrial

130   stable carbon isotopic composition of the dissolved inorganic carbon ($\delta^{13}C_{DIC}$) at 250 m water

131   depth (Eide et al. 2017). Black arrows schematically represent the large-scale geostrophic

132   currents between 100- and 500 m water depth. The dashed line depicts the Subantarctic and

133   Polar Fronts (Orsi et al., 1995). Orange arrows depict the Agulhas leakage rings (adapted

134   from Stramma and England, 1999). BC: Brazil Current; EUC: Equatorial Under Current; MC:

135   Malvinas Current; NBC: North Brazil Current; NECC: North Equatorial Countercurrent; SAC:

136   South Atlantic Current; SEC: South Equatorial Current; SECC: South Equatorial Countercur-

137   rent. b) Western Atlantic Ocean meridional section of salinity (Zweng et al., 2018); c) Western

138   Atlantic Ocean meridional section of the pre-industrial $\delta^{13}C_{DIC}$ (Eide et al., 2017). In both sec-

139   tions, AABW: Antarctic Bottom Water; AAIW: Antarctic Intermediate Water; CDW: Circumpolar

140   Deep Water; NADW: North Atlantic Deep Water; SACW: South Atlantic Central Water. In all

141   panels, purple diamonds indicate sediment cores GL-1248, GL-1180, and GL-1090 (this

142   study), while green triangles indicate the sediment cores M125-95-3 (Campos et al., 2020),

143   GS07-150-17/1GC-A (1GC-A in the figure) (Freeman et al., 2015), M78/1-235-1 (Poggemann

144   et al., 2017), KNR159-5-90GGC (Lund et al., 2015), KNR-159-5-36GGC (Tessin and Lund,

145   2013), and MD02-2588 (Ziegler et al., 2013). The figure was partially generated using the

146   software Ocean Data View (Schlitzer, 2017).

147

148   The global deep ocean circulation can be separated in the upper and lower cells

149   (Toggweiler et al., 2006; Talley, 2013). Over the SO, the westerlies force northward Ekman

150   transport, which is compensated by the upwelling of Circumpolar Deep Water (CDW) in the

151   Antarctic Zone (Marshall and Speer, 2012; Toggweiler and Samuels, 1995). In the upper cell,

152   which is more limited to the Atlantic Ocean, SOIWs composed by the lightest portion of CDW

153   will feed the formation of the NADW in the North Atlantic. In the lower cell, the densest portion

154   of CDW moves towards the Antarctic continental shelf to form Antarctic Bottom Water

155   (AABW), which flows northward, occupying the ocean abyss below approximately 4000 m

156   water depth (Pellichero et al., 2018; Abernathey et al., 2016; Talley, 2013). In the modern

157   ocean, there is an interplay between these two cells (Talley, 2013).

158   The spatial distribution of South Atlantic stable carbon isotopic composition of dis-

159   solved inorganic carbon ($\delta^{13}C_{DIC}$) at 250 m water depth (Fig 1a) reveals the oligotrophic and

160   high $\delta^{13}C_{DIC}$ SASG (warm tones in Fig. 1a), while in the equatorial and eastern tropical Atlantic

161   (Guinea and Angola domes), reduced ventilation and high productivity and remineralization of

162   organic carbon result in $^{13}C_{DIC}$-depleted subsurface waters (cold tones in Fig. 1a). The merid-

163   ional $\delta^{13}C_{DIC}$ section from the western tropical and South Atlantic Ocean (Fig 1c) exhibits the

164   pattern of ^{13}C-depletion at thermocline and intermediate depths in the tropics. Oppo et al.

165   (2018) show that remineralization is responsible for up to 1‰ of $\delta^{13}C_{DIC}$ depletion at thermo-

166   cline and intermediate depth in the western tropical Atlantic. Approximately, 60% of this re-

167   mineralization occurs near the formation site of AAIW, while the rest occurs as AAIW advects

168   northward. The vertical $\delta^{13}C_{DIC}$ profile at about 20°S is marked by a decrease from the oligo-

169   trophic SASG (~1.5 ‰) downward through the SACW and AAIW until reaching the minimum

170   of ~0.7 ‰ at 1300 m water depth, reflecting the influence of Upper Circumpolar Deep Water.

171   Below that, $\delta^{13}C_{DIC}$ increases again due to the $^{13}C_{DIC}$-enriched NADW (~1 ‰) that flows south-

172   ward between 1500 and 4000 m water depth. Finally, in the South Atlantic abyss, the $^{13}C_{DIC}$-

173   depleted AABW (~0.5 ‰) flows northward, underlying NADW.

174   **3. Methods**

175   **3.1. Sediment cores**

176   In this study, we present new data from sediment cores GL-1248 (0°55'20" S,

177   43°24'10" W, 2264 m water depth, 19.29 m long) from the Brazilian equatorial margin, GL-

178   1180 (8°27'18" S, 33°32'53" W, 1037 m water depth, 17.32 m long) from the Brazilian tropical

179   margin and GL-1090 (24°55'12'' S, 42°30'36'' W, 2225 m water depth, 19.14 m long) from the

180   Brazilian subtropical margin (Fig 1). All sediment cores were provided by the Brazilian oil com-

181   pany Petrobras. A visual analysis of the core sections does not indicate any sedimentation

182   disturbance, except for a hiatus between 2.18 and 1.70 m in core GL-1248 (Venancio et al.,

183   2018). The three cores were sampled at 2 cm resolution with sample volume of approximately

184   10 cm^3. Samples were wet-sieved to retain the fraction larger than 63 μm. The retained mate-

185   rial was dried at 50°C for 24 hours and stored in acrylic containers. Foraminifera shells were

186   handpicked using a binocular microscope.

3.2. Age model

188   We used the published age model of core GL-1248 (Venancio et al., 2018), based on

189   twelve calibrated radiocarbon ages and the visual alignment of its Ti/Ca ratio to the Greenland

190   stable oxygen isotope (δ^{18}O) record (NGRIP members, 2004), using the extended Greenland

191   Ice Core Chronology (GICC05modelext) (Wolff et al., 2010). This alignment assumes that

192   Ti/Ca peaks resulting from increased precipitation in the northeast Brazilian region correspond

193   to North Atlantic cold events (e.g., Zhang et al., 2017). GL-1248 was sampled relatively close

194   to the Parnaíba River mouth and was significantly influenced by terrigenous input during peri-

195   ods of low sea levels and high precipitation periods in northeastern Brazil (Venancio et al.,

196   2018). The age model was built using the software Clam 2.2 (Blaauw, 2010), with GL-1248

197   spanning the last 124 ka, and was described in detail by Venancio et al. (2018).

198   The age model of core GL-1180 was published by Nascimento et al. (2021) and is

199   based on six calibrated radiocarbon ages (Supporting Information, Table S1) and the align-

200   ment of the benthic δ^{18}O record of *Cibicides* spp. with the global δ^{18}O stack LR04 (Lisiecki and

201   Raymo, 2005) (Table S2 and Fig. S1). The benthic δ^{18}O tie point uncertainties were calculated

202   following the recommendations by Govin et al. (2015). The calculation used the uncertainties

203   of the reference stack and of the alignment procedure, as well as the resolutions of the refer-

204   ence stack and of the target record. Radiocarbon ages were calibrated using the IntCal13

205   calibration curve (Reimer et al., 2013), with a reservoir effect of 400 ± 200 without any addi-

206   tional local reservoir effect. The age model (Fig. S1) was built using the software Bacon v 2.3

207   (Blaauw and Christen, 2011); it shows that sediment core GL-1180 spans the last 300 kyr.

208   More details about the age model can be found in Nascimento et al. (2021).

209   For core GL-1090, we use the age model previously published by Santos et al. (2017)

210   and improved by Ballalai et al. (2019) and Santos et al. (2020). It is based on ten calibrated

211   radiocarbon ages and the alignment of its benthic $\delta^{18}O$ record of (*Cibicides wuellerstorfi*) with

212   the benthic $\delta^{18}O$ records from the reference curves LR04 (Lisiecki and Raymo, 2005) and

213   MD95-2042 (Govin et al., 2014). The age model was built using the software Bacon v 2.3

214   (Blaauw and Christen, 2011), with GL-1090 covering the last 182 kyr.

215   **3.3. Foraminifera stable carbon isotopes ($\delta^{13}C$) analysis**

216   Our $\delta^{13}C_{DIC}$ reconstruction of SACW is based on the $\delta^{13}C$ data from thermocline-

217   dwelling foraminifera *Neogloboquadrina dutertrei* (GL-1248), *Globorotalia truncatulinoides*

218   (dextral) (GL-1180), and *Globorotalia inflata* (GL-1090). The apparent calcification depth

219   (ACD) of *N. dutertrei* was estimated to be 150 m in the region of core GL-1248 (Venancio et

220   al. 2018), in line with previous estimates in the tropical Atlantic (Cléroux et al., 2013; Farmer

221   et al., 2007; Steph et al., 2009). *G. truncatulinoides* presents a wide vertical migration range

222   during its life cycle but primarily calcifies at the main thermocline (Steph et al., 2009; Regen-

223   berg et al., 2009; Cléroux et al., 2007; LeGrande et al., 2004), which is consistent with an ACD

224   of ~250 m in the region of core GL-1180 (Nascimento et al., 2021). In the western South At-

225   lantic, the *G. inflata* ACD stably ranges from 350 to 400 m water depth (Groeneveld and

226   Chiessi, 2011).

227   Between 5 and 10 shells of *N. dutertrei* (350-415 µm), *G. truncatulinoides* (dextral;

228   300-425 µm), and *G. inflata* (250-300 µm) were handpicked from samples of cores GL-1248,

229   GL-1180, and GL-1090, respectively. The sampling resolution varied between 2 and 4 cm

230   downcore.

231   Our reconstruction of seawater $\delta^{13}C$ for intermediate depth is based on $\delta^{13}C$ from ben-

232   thic foraminifera *Cibicides* spp. from core GL-1180 (1037 m water-depth). To do so, between

233   5 and 10 shells of *Cibicides* spp. (300-350 µm), composed by *Cibicides pachyderma, Cibicides*

234   *refulgens,* and *Cibicides kullenbegi* (Supporting Information, Text S1), were handpicked at 4

235   cm resolution.

236   Analyses of planktonic foraminifera from the cores GL-1248 and GL-1090, and benthic

237   foraminifera from GL-1180 were carried out in the Center for Marine Environmental Sciences

238   (MARUM), University of Bremen, Germany, using a Finnigan MAT 251 isotope ratio mass

239   spectrometer (IRMS) equipped with an automated carbonate preparation device (Kiel I). Data

240   were calibrated against the in-house standard (Solnhofen limestone), and the standard devi-

241   ation of the in-house standard over the measurement period was 0.03 ‰. Analyses of plank-

242   tonic foraminifera from core GL-1180 were performed in the Paleoceanography and Paleocli-

243   matology Laboratory, University of São Paulo, Brazil, using a Thermo^{TM} Scientific MAT 253

244   IRMS coupled to a Thermo™ Kiel IV automated carbonate preparation device (Kiel IV) (Crivel-

245   lari et al., 2021). Data were calibrated against the NBS 19 standard. The standard deviation

246   of NBS 19 over the measurement period was 0.02 ‰. All data are presented in parts per

247   thousand (‰) relative to the Vienna Pee Dee belemnite (VPDB).

248   **4. Results**

249   The $\delta^{13}C$ of *N. dutertrei* (GL-1248) ranges between 1.11 and 2.29 ‰ (mean 1.70 ±

250   0.17 ‰), while the $\delta^{13}C$ range is from 0.23 to 1.93 ‰ (mean 1.21 ± 0.21 ‰) for *G. truncatuli-*

251   *noides* (GL-1180), and between 0.06 to 1.47 ‰ (mean 0.80 ± 0.19 ‰) for *G. inflata* (GL-1090)

252   (Fig. 2). Planktonic $\delta^{13}C$ records from all studied cores present a similar pattern with remark-

253   able negative excursions during glacial terminations that only recover after the onset of the

254   following interglacial period (Fig. 2). The records show little difference between glacial and

255   interglacial $\delta^{13}C$ values. A prominent negative excursion is also observed during the transition

256   between Marine Isotope Stage (MIS) 4 and MIS 3. In general, the benthic $\delta^{13}C$ record from

257   core GL-1180 is similar to the thermocline $\delta^{13}C$ records (Fig 2a). The average benthic $\delta^{13}C$ is

258   0.64 ± 0.17 ‰, and the values range between 0.02 and 1.49 ‰, similar to *G. inflata* $\delta^{13}C$ from

259   core GL-1090.

260   Termination IIIb (Fig 2d) is only recorded in sediment core GL-1180, which covers the

261   last 300 kyr. *G. truncatulinoides* and *Cibicides* spp. $\delta^{13}C$ records show a drop of 0.4 and 0.5

262   ‰, respectively, relative to MIS 8. $\delta^{13}C$ minima are also observed during Termination IIIa at

263   the transition between MIS 7d and MIS 7c. A more pronounced δ^{13}C minimum occurred during

264   Termination II (Fig 2c), when *G. truncatulinoides* and *G. inflata* δ^{13}C values drop by ~0.8 and

265   ~0.4 ‰, respectively. Similarly, during Termination II, the benthic δ^{13}C record dropped by ~0.6

266   ‰ relative to MIS 6 (Fig 2c). The *N. dutertrei* δ^{13}C record spans the last 124 ka only, and its

267   oldest samples indicate that δ^{13}C is recovering from a minimum of at least 1.40 ‰ to reach

268   interglacial values of ~1.8 ‰ at 121 ka. All records show negative δ^{13}C excursions during

269   MIS4/3 transition. These excursions are equivalent to those observed during glacial termina-

270   tions. The largest drops are exhibited in *N. dutertrei* (GL-1248) and *G. inflata* (GL-1090), where

271   δ^{13}C values decrease by ~0.5 ‰. *G. truncatulinoides* and *Cibicides spp.* (GL-1180) show a

272   δ^{13}C decrease of ~0.3 ‰. During Termination I, *G. inflata* and *G. truncatulinoides* δ^{13}C drops

273   approximately 0.4 ‰ relative to MIS 2 (Fig. 2b). *G. truncatulinoides* δ^{13}C presents several

274   short-lived δ^{13}C drops within a broad negative excursion that started at ~18 ka. For *G. inflata*

275   and *G. truncatulinoides* records, fully interglacial values are reached at ~7 ka. GL-1248 pre-

276   sents a hiatus between 29 and 14 ka, but we note that δ^{13}C is low at the end of Termination I

277   and reaches interglacial values in the mid-Holocene. During Termination I, the δ^{13}C record of

278   *Cibicides* spp. shows two negative excursions of up to ~0.4 ‰ relative to the Last Glacial Max-

279   imum (LGM) (Fig 2b).
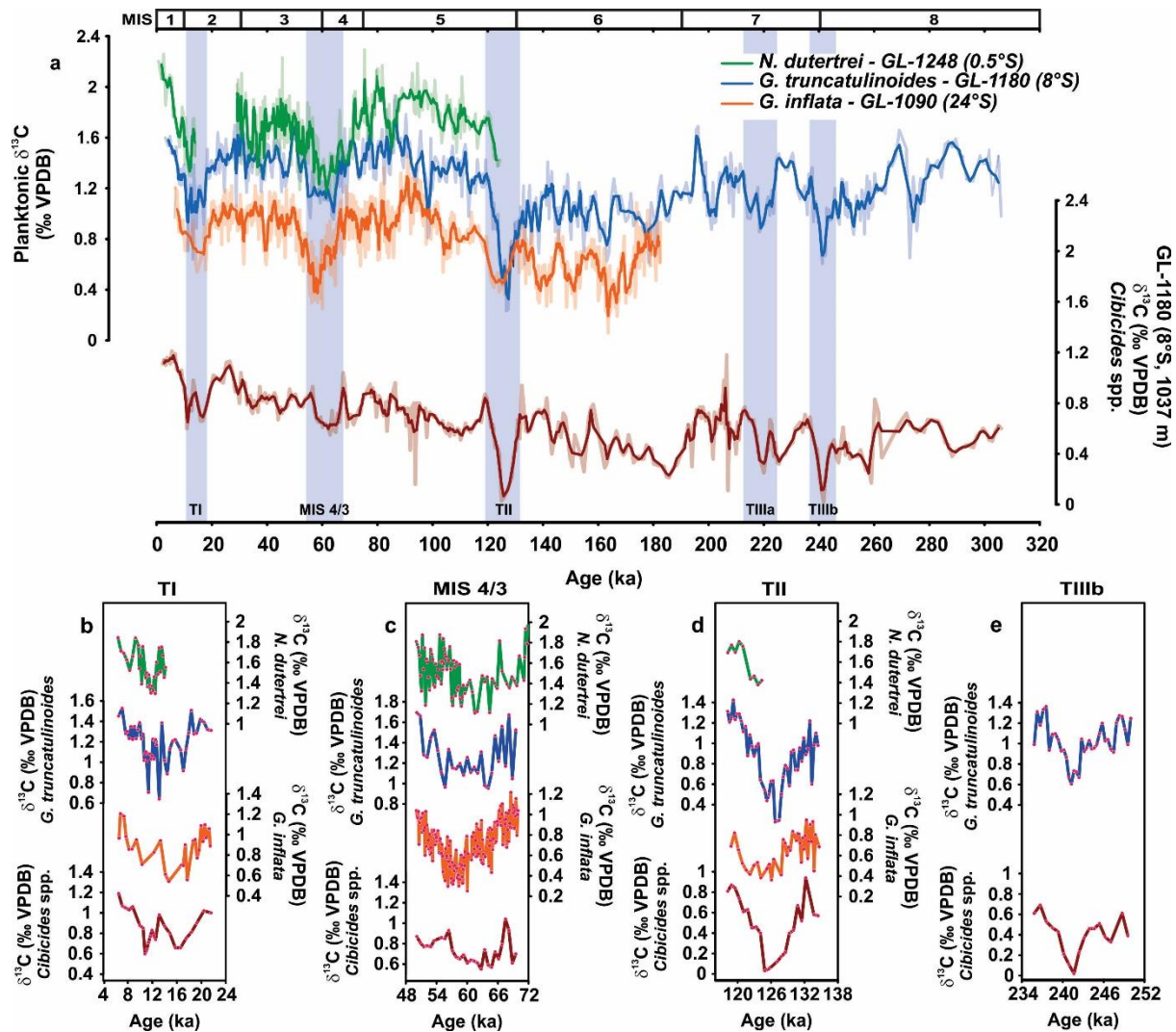
Figure 2. Carbon isotopic composition (δ^{13}C) of planktonic and benthic foraminifera analyzed in this study. a) δ^{13}C of *Neogloboquadrina dutertrei* (GL-1248, green line), *Globorotalia truncatulinoides* (GL-1180, blue line), *Globorotalia inflata* (GL-1090, orange line), *Cibicides* spp. (GL-1180, dark-red line). Blue bars indicate δ^{13}C minimum events during glacial terminations and the Marine Isotope Stage (MIS) 4/3 transition. Dark colored lines depict the three points running average, while light colored lines depict the original data. Zooms of deep-dwelling and benthic δ^{13}C records for b) zoom into Termination I (TI); c) zoom into MIS4/3 transition; d) zoom into Termination II (TII); e) zoom into Termination IIIb (TIIIb) colors as in a). MIS are indicated at the top of panel a.

5. Discussion

5.1. δ^{13}C values of planktonic foraminifera

13

292   We present δ¹³C values of three deep-dwelling planktonic foraminifera species in order

293   to reconstruct $\delta^{13}C_{DIC}$ of thermocline waters in the western South Atlantic. Although δ¹³C of

294   the calcite reflects $\delta^{13}C_{DIC}$, it is not in isotopic equilibrium with seawater (Ravelo and Hillaire-

295   Marcel, 2007). Offsets between $\delta^{13}C_{DIC}$ and δ¹³C of calcite are related to abiotic kinetic frac-

296   tionation, which causes an offset of 1.0 ± 0.2 ‰ (Romanek et al., 1992), changes in foraminif-

297   era metabolic rate (Bemis et al., 2000), seawater carbonate ion concentration (Spero et al.,

298   1997; Wilke et al., 2006), and photosymbiosis (Spero and Deniro, 1987). The δ¹³C from *G.*

299   *truncatulinoides* and *G. inflata* is known to be dependent on shell size (Birch et al., 2013;

300   Friedrich et al., 2012; Elderfield et al., 2002). This is likely an effect of high metabolic rates of

301   individuals in early ontogenetic stages but analyzing shells larger than 250 μm largely avoids

302   this effect (Birch et al., 2013; Friedrich et al., 2012). Even so, the δ¹³C average of 11 core-tops

303   (1.0 ‰ ± 0.2) from the western South Atlantic (Chiessi et al., 2007) shows that *G. inflata* is

304   ~0.5 ‰ lighter than the pre-industrial $\delta^{13}C_{DIC}$ provided by Eide et al. (2017) in the same region

305   between 350 to 400 m water depth. The same result was found in sediment trap samples from

306   the Cape Basin (Wilke et al., 2006), suggesting that this offset is a widespread feature of this

307   species in the South Atlantic. In the opposite direction, plankton tow samples from the equa-

308   torial Atlantic reveal that *N. dutertrei* δ¹³C is about 0.5 ‰ higher than $\delta^{13}C_{DIC}$ (Mulitza et al.,

309   1999). Therefore, δ¹³C differences or similarities between foraminifera species may not only

310   result from habitat depth but also from offsets between $\delta^{13}C_{DIC}$ and δ¹³C of calcite. Yet, these

311   effects mostly affect the absolute δ¹³C values and are not expected to influence temporal

312   changes in the downcore records, which is the central aspect discussed here.

313   The δ¹³C of *G. truncatulinoides* is considered a robust proxy for nutrient content in the

314   thermocline (Mulitza et al., 1998). *G. truncatulinoides* δ¹³C record from GL-1180 presents a

315   positive offset of ~0.5 ‰ relative to the same species in the Agulhas Plateau (MD02-2588,

316   41°S) (Ziegler et al., 2013) and in the western South Pacific (ODP1123, 41°S) (Hu et al., 2020)

317   (Fig. 3b). Since sites MD02-2588 and ODP1123 are near central waters formation latitudes,

318   we would presume their *G. truncatulinoides* δ¹³C values to be higher than in the aged central

319   waters in the tropics. The positive offset of *G. truncatulinoides* δ¹³C in the tropics relative to

14

320   the subtropics may be related to ecological distinctions between organisms living in these

321   regions, morphotype (dextral or sinistral), and the shell size. In the stratified tropical Atlantic,

322   the ACD range of *G. truncatulinoides* is estimated to extend from the base of the seasonal

323   thermocline to ~400 m water depth (Mulitza et al., 1997). In the subtropics, this species ex-

324   tends its life cycle from the weakly stratified ocean surface to ~800 m water depth (Mulitza et

325   al., 1997; Ujiié et al., 2010; Hu et al., 2020). In fact, this large difference in the depth range

326   may favor the *G. truncatulinoides* secondary calcite crust, which forms deeper in the water

327   column (Mulitza et al., 1997), to record lower δ^{13}C values in the subtropics relative to the trop-

328   ical ocean. Additionally, in contrast to Hu et al. (2020) and Ziegler et al. (2013) who analyzed

329   the sinistral morphotype of *G. truncatulinoides*, we used the *G. truncatulinoides* dextral. In-

330   deed, it was suggested that the dextral morphotype shows a shallower ACD and prefers a

331   more stratified thermocline than the sinistral (Feldmeijer et al., 2014; Ujiié et al., 2010). Be-

332   sides, the size fraction analyzed in our study is larger than in the aforementioned studies,

333   reducing the effect of metabolic rate on the δ^{13}C of calcite (Birch et al., 2013; Friedrich et al.,

334   2012). Mixing with high δ^{13}C of SASG waters (Fig. 1a, c) may also contribute to increasing

335   the thermocline δ^{13}C in the tropics relative to the subtropics (Fig. 3b).

336   Despite the difference in location and species measured within GL-1090 (i.e. *G. inflata*

337   from the SASG) to those of Ziegler et al. (2013) and Hu et al. (2020) (i.e. G. *truncatulinoides*

338   from Agulhas Plateau and western South Pacific, respectively), the three records present sim-

339   ilar δ^{13}C values (Fig. 3b). We ascribe this similarity to the negative ~0.5 ‰ offset of *G. inflata*

340   δ^{13}C relative to $\delta^{13}C_{DIC}$ (Wilke et al., 2006) and to the deep ACD of *G. inflata* in the western

341   South Atlantic (Groeneveld and Chiessi, 2011). The higher averaged δ^{13}C values observed in

342   the *N. dutertrei* record (GL-1248) (Fig. 2a) may reflect the shallow habitat within the thermo-

343   cline and the additional positive offset (0.5 ‰) relative to $\delta^{13}C_{DIC}$ observed in the equatorial

344   Atlantic (Mulitza, 1999).
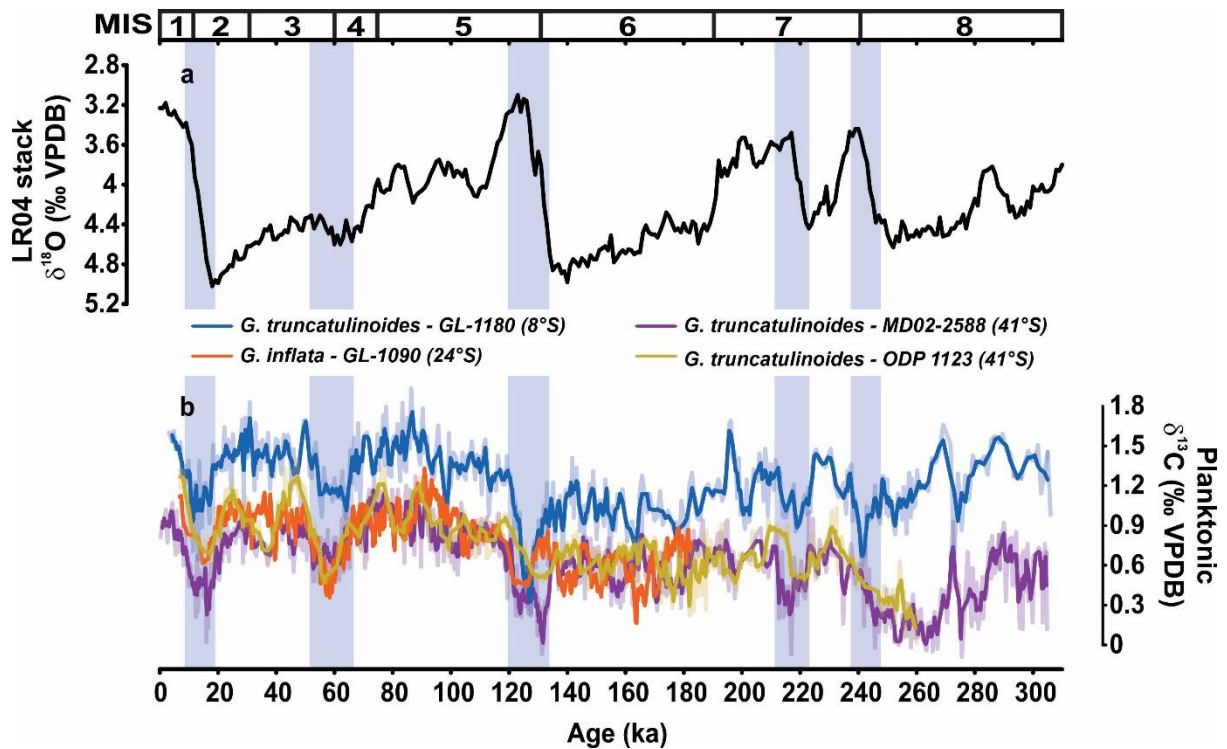
Figure 3. Stable carbon isotopic (δ¹³C) records presented in this study compared with published thermocline (see locations in Fig. 1) records. a) LR04 global oxygen stable isotopic (δ¹⁸O) stack (Lisiecki and Raymo, 2005). b) δ¹³C of *Globorotalia truncatulinoides* from the western tropical South Atlantic (GL-1180, blue line), *Globorotalia inflata* from the western subtropical South Atlantic (GL-1090, orange line), *G. truncatulinoides* from the Agulhas Plateau (MD02-2588, purple line) (Ziegler et al., 2013), and *G. truncatulinoides* from the western South Pacific (ODP1123, dark yellow) (Hu et al., 2020). Dark colored lines depict the three points running average, while light colored lines depict the original data. Blue bars indicate δ¹³C minimum events during glacial terminations and the Marine Isotope Stage (MIS) 4/3 transition. MIS are indicated at the top of the panel a.

5.2. Mechanisms behind δ¹³C minimum events at thermocline and intermediate depth

5.2.1. The oceanic tunnel hypothesis

The deglacial δ¹³C minimum events shown by our records can be potentially explained by the transport of ¹³C-depleted carbon from the deep ocean to the SO surface and its equatorward advection by SOIWs (Spero and Lea, 2002), the so-called "oceanic tunnel" hypothesis (e.g., Pena et al., 2013), in reference to Liu and Yang (2003). The deep ocean is hypothesized

16

362   as the main sink of atmospheric CO_2 during glacial periods. During glacial terminations, the

363   SO warmed (WAIS members, 2013; Barker et al. 2009), the sea-ice cover shrank (WAIS mem-

364   bers, 2013; Gersonde and Zielinski, 2000), and the Southern Hemisphere westerlies are

365   thought to have shifted southward and strengthened (Menviel et al., 2018; Toggweiler et al.,

366   2006). The reduction in brine rejection due to reduced sea-ice cover, together with the stronger

367   westerlies, resulted in the breakup of deep ocean stratification and enhancement of its venti-

368   lation (Du et al., 2018; Basak et al., 2018; Skinner et al., 2010), transporting nutrient-rich and

369   ^{13}C-depleted waters from the deep ocean to the SO surface (Anderson et al., 2009; Ziegler et

370   al., 2013). Finally, the low $\delta^{13}C$ signal was transmitted northward by the SOIWs (Spero and

371   Lea, 2002). Spero and Lea (2002) hypothesized a correspondence between the $\delta^{13}C_{DIC}$ sig-

372   nals of central waters and AAIW for the "oceanic tunnel" hypothesis to be valid. Indeed, our

373   planktonic records share a similar structure with the benthic record from GL-1180 (Fig 2a).

374   Since modern SACW and AAIW have a similar source and formation mechanism (Pellichero

375   et al., 2018; Abernathey et al., 2016; Tomczak and Godfrey, 1994), our results, at least theo-

376   retically, corroborate the subsurface link between the SO and low latitudes, which resulted in

377   the $\delta^{13}C$ minima observed in the western South Atlantic over the last three glacial terminations.

378   Ninnemann and Charles (1997) speculated that regions with little or no influence of

379   SOIWs should have a different $\delta^{13}C$ signal from that seen in the Southern Hemisphere. How-

380   ever, $\delta^{13}C$ minima have also been found in thermocline records of the subtropical North Atlan-

381   tic, far from the influence of SOIWs (Lynch-Stieglitz et al., 2019). Besides, at intermediate

382   depth, the occurrence of these events was limited to the tropical (e.g., Poggemann et al., 2017;

383   Freeman et al., 2015; Arz et al., 1999) and North Atlantic (e.g., Oppo et al., 2015; Rickaby and

384   Elderfield, 2005). In contrast, intermediate depth $\delta^{13}C$ records from subtropical latitudes of the

385   southern Brazilian margin (~27°S) revealed no evidence of ^{13}C-depleted northward-flowing

386   AAIW during the last glacial termination (Lund et al., 2015; Tessin and Lund, 2013; Oppo and

387   Horowitz, 2000). Analogous results were reported at intermediate depth of the eastern sub-

388   tropical Pacific Ocean (Pahnke and Zahn, 2005; Bostock et al., 2004). Additionally, intermedi-

389   ate depth $\Delta^{14}C$ records (a proxy of water mass ventilation) from the SO do not point to a poorly

390 ventilated AAIW during the last termination (Burke and Robinson, 2012). Similarly, $\Delta^{14}C$ rec-

391 ords from the southern Brazilian margin (Sortor and Lund, 2011) and equatorial Atlantic (Clé-

392 roux et al., 2011; Chen et al., 2020) give support to persistent well-ventilated thermocline and

393 intermediate waters during Termination I. Together, stable and radiogenic carbon isotopes,

394 suggest that the SOIWs were not a pathway for aged and ^{13}C-depleted carbon accumulated

395 in the deep ocean during glacial periods. Therefore, the "oceanic tunnel" mechanism is not

396 expected to have played a major role in causing the $\delta^{13}C$ minimum events in our records and

397 in other records from the tropical and North Atlantic.

398 *5.2.2. The thermodynamic ocean-atmosphere isotopic equilibration hypothesis*

399 $\delta^{13}C$ minimum events in the atmosphere (Fig. 4a) (Eggleston et al., 2016; Schmitt et

400 al., 2012) have also been ascribed to the enhanced upwelling around the Antarctica and the

401 outgassing of ^{13}C-depleted CO_2 from the SO ocean surface (Schmitt et al., 2012). Previous

402 studies have suggested that the atmosphere can work as a bridge, globalizing its low atmos-

403 pheric $\delta^{13}C$ signal in the upper ocean through the temperature-mediated ocean-atmosphere

404 isotopic equilibration, also named thermodynamic equilibration (Shao et al., 2021; Lynch-

405 Stieglitz et al., 2019). Accordingly, the deglacial $\delta^{13}C$ minima observed in thermocline and in-

406 termediate depths in the western South Atlantic (Fig. 2a) may have been caused by the ther-

407 modynamic equilibration in the formation regions of the water masses that fill these depths

408 (Lynch-Stieglitz et al. 2019; Lynch-Stieglitz et al., 1995; Lynch-Stieglitz and Fairbanks, 1994;

409 Broecker and Maier-Reimer, 1992). This hypothesis explains, for example, the presence of

410 low $\delta^{13}C$ signal in oceanic regions where the nutrient concentrations are thought to have been

411 always low and in regions that are not affected by the northward flowing SOIWs, as the North

412 Atlantic (Lynch-Stieglitz et al., 2019; Ninnemann and Charles, 1997).

413 Empirical experiments indicate that the $\delta^{13}C$ at the ocean surface tend to be 0.1 ‰

414 higher relative to the atmospheric value per degree of cooling (Zhang et al., 1995). To estimate

415 the influence of the thermodynamic equilibration in the western South Atlantic, we used the

416 sea surface temperature (SST) record from site GL-1090 (Fig. 4b) (Santos et al., 2017) and

417   the isotopic composition of atmospheric CO_2 over the last 150 kyr (Fig. 4a) (Eggleston et al.,

418   2016) to estimate the predicted $\delta^{13}C_{DIC}$ at the ocean surface. We applied the thermodynamic

419   isotopic-equilibrium equation published by Zhang et al. (1995), where $\varepsilon_{DIC-g} = (10.51 \pm 0.05)$

420   - $(0.105 \pm 0.002) \times T$. This equation was derived from direct measurement of the isotope

421   fractionation between DIC of seawater and atmospheric CO_2 for a temperature and carbonate

422   ion fraction range of 5 to 25°C and 0.05 to 0.2, respectively (Zhang et al., 1995). By using the

423   SST record from GL-1090 (24°S), we assume that this region in the South Atlantic Subtropical

424   Gyre is representative of where the ocean exchanges CO_2 with the atmosphere and that these

425   surface waters will be eventually pumped to the South Atlantic thermocline. It is also notewor-

426   thy that this estimate only assumes the effect of thermodynamic equilibration on the $\delta^{13}C_{DIC}$.

427   The predicted $\delta^{13}C_{DIC}$ (Fig. 4d) strongly resembles the *G. inflata* $\delta^{13}C$ record (Fig. 4c), showing

428   similar millennial and long-term variations and with similar magnitude of $\delta^{13}C$ drops to those

429   presented by our planktonic foraminifera record. Therefore, we argue that the ocean-atmos-

430   pheric thermodynamic equilibration can substantially modulate the thermocline $\delta^{13}C$ in the

431   western South Atlantic in orbital time-scales. Indeed, this result agrees with recent numerical

432   modeling, which demonstrates that thermodynamic equilibration dominates the upper ocean

433      $\delta^{13}C_{DIC}$ minimum anomaly during the last glacial termination (Shao et al., 2021). Previous mod-

434   eling outputs also support the role of thermodynamic equilibration on the upper ocean $\delta^{13}C_{DIC}$

435   (Menviel et al., 2018; Schmittner and Lund, 2015).

436   The average of our predicted $\delta^{13}C_{DIC}$ record (1.48 ‰) is ~0.7 ‰ higher relative to the

437   average of our *G. inflata* $\delta^{13}C$ record (0.8 ‰). This result is expected since $\delta^{13}C_{DIC}$ was pre-

438   dicted for the ocean surface. Additionally, as mentioned in section 5.1., *G. inflata* $\delta^{13}C$ shows

439   a negative offset relative to $\delta^{13}C_{DIC}$ (e.g., Wilke et al., 2006). Besides, the thermocline $\delta^{13}C_{DIC}$

440   in the western tropical and South Atlantic is also affected by the $\delta^{13}C$ signal of the remineral-

441   ized and preformed components of DIC (Oppo et al., 2018).

442   Both the predicted and the *G. inflata* $\delta^{13}C$ records show a remarkable drop (~0.5 ‰)

443 during the MIS 4/3 transition (Fig. 4c, d). This drop is similar to that found in $\delta^{13}C$ of atmos-

444 pheric CO_2 (~0.5 ‰) (Eggleston et al., 2016). The MIS 4/3 transition can be considered an

445 unfinished glacial termination following the maximum extension of Southern Hemisphere glac-

446 iers at ~65 ka (MIS 4) (Schaefer et al., 2015). Indeed, several lines of evidence point to the

447 Southern Hemisphere under full glacial conditions during MIS 4 (Kohfeld and Chase, 2017;

448 Schaefer et al., 2015; Barker and Diz, 2014). During MIS 4/3 transition, Antarctica showed a

449 substantial warming, equivalent to the beginning of a full glacial termination (Wolff et al., 2009).

450 In addition, the atmospheric CO_2 concentration increased by ~30 ppm (Bereiter et al. 2012).

451 We argue that the climatic conditions around MIS 4/3 transition were akin to the beginning of

452 a full termination. Consequently, the enhancement of the SO upwelling during this transition

453 resulted in the transfer of ^{13}C-depleted carbon from the deep ocean to the atmosphere, which

454 ultimately imprinted its signal in the upper ocean.

455   A reduction of the biological pump efficiency may also have contributed to the negative

456 $\delta^{13}C$ anomaly in the thermocline during glacial terminations, due to the accumulation of iso-

457 topically light carbon in the upper ocean (Lund et al., 2019; Hertzberg et al., 2016; Schmittner

458 and Lund, 2015). However, $\delta^{13}C$ depletions are observed in regions where changes in the

459 biological pump are not expected to have occurred, e.g., site GL-1180 (8°S), which is in the

460 northern portion of the oligotrophic South Atlantic Subtropical Gyre. We also found thermocline

461 $\delta^{13}C$ depletions in regions where the primary productivity is thought to have increased during

462 the last termination, as indicated by Pereira et al. (2018) for the region of sediment core GL-

463 1090 (24°S). However, a weaker biological pump at the Subantarctic Zone (SAZ), due to re-

464 duced dust-borne iron supply during Termination I (Martínez-García et al., 2014; Jaccard et

465 al., 2013), may have caused the advection of ^{12}C-enriched waters to the western South Atlan-

466 tic. These changes in the biological pump at the SAZ can be particularly relevant to the ther-

467 mocline $\delta^{13}C_{DIC}$ depletion in the domain of SAMW, but it would have minimal influence on the

468 thermocline $\delta^{13}C$ minima seen in the Northern Hemisphere (e.g., Lynch-Stieglitz et al., 2019).

469   Although the thermodynamic equilibration may have provided a substantial contribu-

470   tion to the thermocline $\delta^{13}C_{DIC}$ minimum during glacial terminations, the absence of a ^{13}C-

471   depleted signal at intermediate depth in the South Brazilian margin (27°S) (Tessin and Lund,

472   2013; Lund et al., 2015) implies that the isotopic equilibration through southern-sourced wa-

473   ters did not imprint the low $\delta^{13}C_{DIC}$ signal at intermediate depth of the South Atlantic. Alterna-

474   tively, the signal of the thermodynamic equilibration in AAIW may have been overcome by

475   other processes. For example, a weaker biological pump at the SAZ may have reduced the

476   export of organic matter and its remineralization at intermediate depth, thus causing the in-

477   crease in the $\delta^{13}C_{DIC}$ observed in the AAIW domain (Hertzberg et al., 2016). Such a hypothe-

478   sized reduction of the biological pump at the SAZ agrees with the role of the regeneration of

479   organic matter in modulating the $\delta^{13}C_{DIC}$ signal at intermediate depth of the tropical and South

480   Atlantic, as shown by Oppo et al. (2018).

481   Therefore, in agreement with previous studies (e.g., Shao et al., 2021; Lynch-Stieglitz

482   et al., 2019) we suggest that the atmosphere acted as a bridge during the early deglaciation,

483   spreading the $\delta^{13}C$ minimum signal globally in the upper ocean. Although thermodynamic equi-

484   libration may have modulated the $\delta^{13}C_{DIC}$ minimum events, changes in preformed and remin-

485   eralized components of DIC can also affect $\delta^{13}C_{DIC}$, particularly in the domain of SAMW (Oppo

486   et al., 2018). Finally, in the South Atlantic, the signal of thermodynamic equilibration was

487   mostly seen in the thermocline so that an alternative mechanism and/or pathway is warranted

488   to explain the $\delta^{13}C$ minimum events observed in the benthic $\delta^{13}C$ record from GL-1180 (1037

489   m, 8° S).
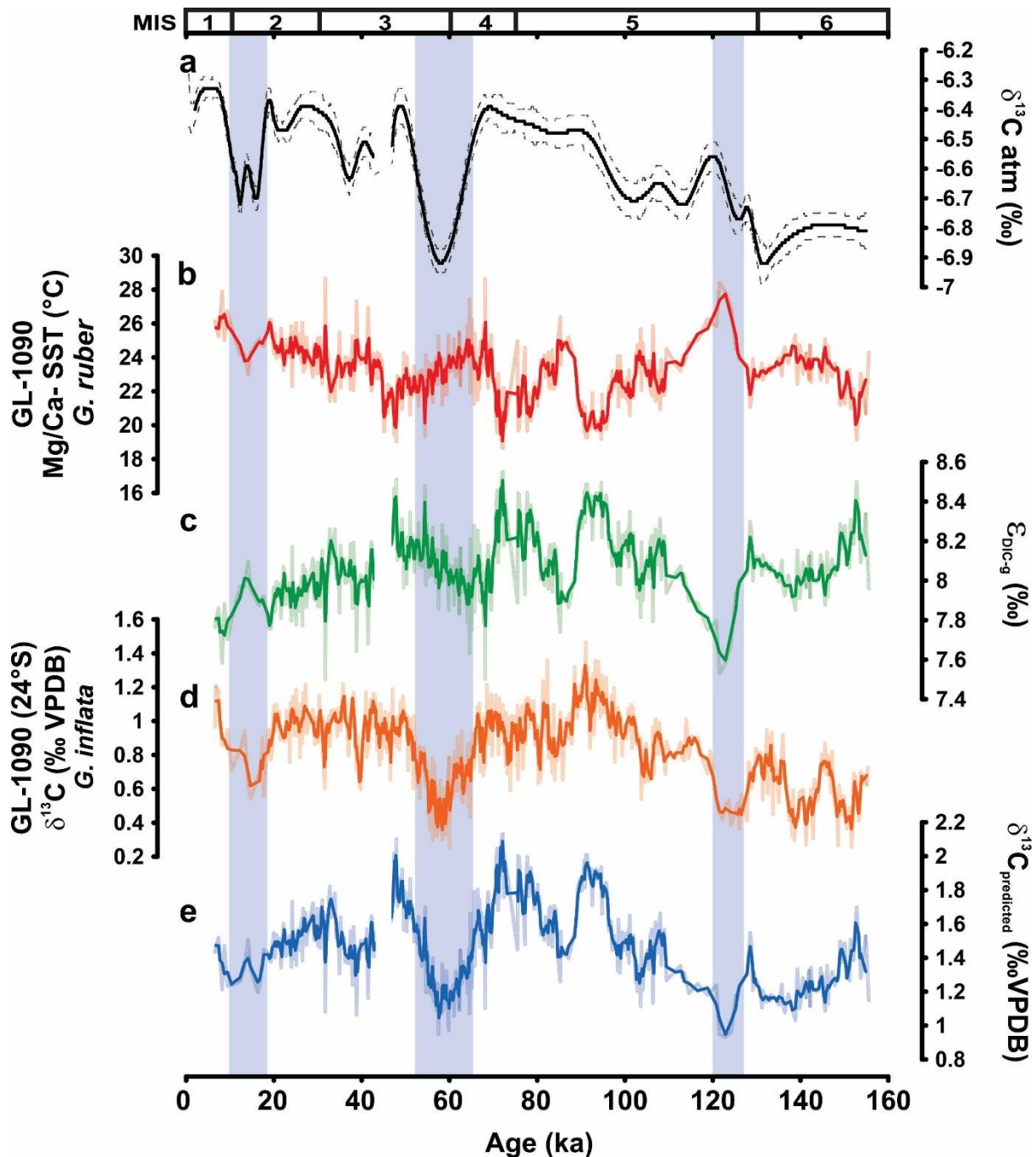
Figure 4. Effect of temperature dependent ocean-atmosphere isotopic equilibration on the stable carbon isotope ratio of the dissolved inorganic carbon ($\delta^{13}C_{DIC}$) of ocean surface in site GL-1090. a) Monte Carlo cubic spline average of atmospheric $\delta^{13}C$ over the last 150 kyr (Eggleston et al., 2016); b) Mg/Ca based sea surface temperature from sediment core GL-1090 (Santos et al. 2017), SST was recalculated using Mg/Ca-temperature equation from Gray and Evans (2019). c) The ^{13}C fractionation between ocean DIC and atmosphere CO_2 calculated using the equation from Zhang et al. (1995). d) $\delta^{13}C$ of *Globorotalia inflata* from site GL-1090

498　(this study). e) The predicted δ¹³C$_{DIC}$ of ocean surface assuming the thermodynamic ocean-

499　atmosphere isotopic equilibration. Bars indicates times synchronic δ¹³C drops in the predicted

500　δ¹³C$_{DIC}$ and *G. inflata* δ¹³C. The thick lines in panels b, c, d, and e depict 3-points running

501　averages.
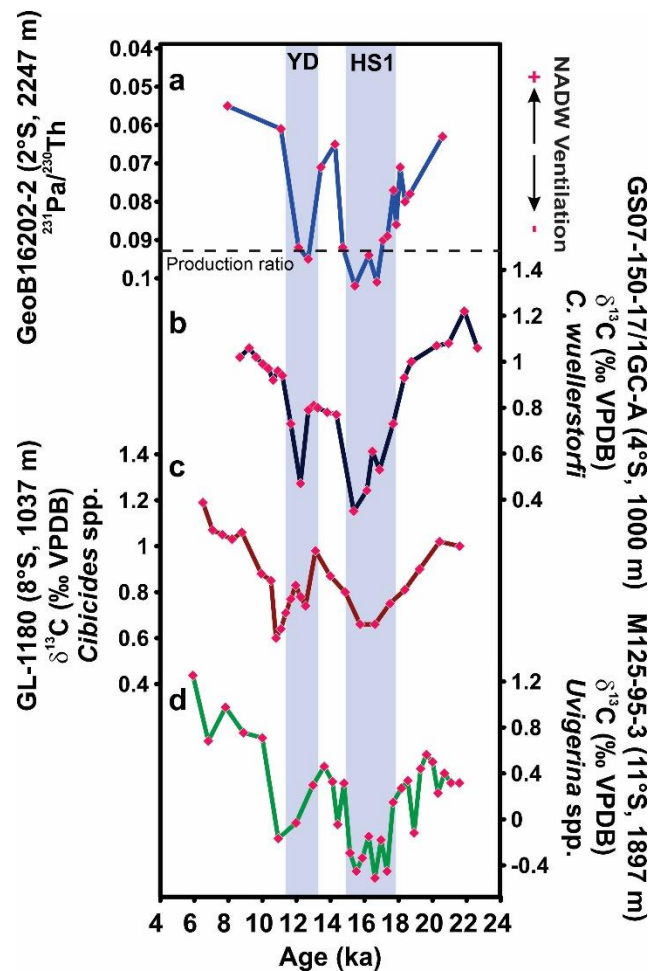
502

503　**Figure 5.** Comparison between the stable carbon isotopic composition (δ¹³C) of benthic foram-

504　inifera from intermediate and mid-depth of the South Atlantic and radiochemical data from the

505　North Atlantic. a) ²³¹Pa/²³⁰Th record from sediment core GeoB16206-1 (Mulitza et al. 2017).

506　Note inverted y axis. b) Benthic δ¹³C from sediment core GS07-150-17/1GC-A (Freemann et

507　al., 2015). c) Benthic δ¹³C of sediment core GL-1180 (this study). d) Benthic δ¹³C of sediment

508　core M125-95-3 (Campos et al., 2020). Blue bars indicate Heinrich Stadial 1 (HS1) and the

509　Younger Dryas (YD).

510   5.2.3. $\delta^{13}C$ minimum events at intermediate depth of the tropical Atlantic: the AMOC slowdown

511   hypothesis

512   As discussed in sections 5.2.1 and 5.2.2, neither the "oceanic tunnel" nor thermody-

513   namic equilibration through southern-sourced waters can explain the $\delta^{13}C$ minimum events

514   observed in our GL-1180 benthic $\delta^{13}C$ record. Here we point to a North Atlantic origin of $\delta^{13}C$

515   minimum events at the intermediate depth of the tropical Atlantic. Over the last glacial termi-

516   nation, ^{13}C-depleted waters have been observed in the mid-depth of the North, tropical, and

517   South Atlantic (Campos et al., 2020; Lacerra et al., 2017; Voigt et al., 2017; Oppo et al., 2015;

518   Lund et al., 2015; Tessin and Lund, 2013). This depletion is likely linked to the reduced NADW

519   ventilation rate during Heinrich Stadial 1 and the Younger Dryas, resulting in the accumulation

520   of respired carbon at mid-depth of the Atlantic Ocean (Lacerra et al., 2017; Schmittner and

521   Lund, 2015). Indeed, reduced NADW ventilation rate is supported by $^{231}Pa/^{230}Th$ values (Fig.

522   5a) from mid-depth of the Atlantic Ocean (e.g., Mulitza et al. 2017; Voigt et al. 2017). Accord-

523   ingly, this mid-depth ^{13}C-depleted signal could have affected intermediate depth (~1000 m)

524   $\delta^{13}C_{DIC}$ signal at the Brazilian equatorial margin during Termination I, as observed in benthic

525   $\delta^{13}C$ record (Fig. 5b) from site GS07-150-17/1GC-A (Fig. 1) (Freeman et al., 2015).

526   Numerical modeling supports a decrease of $\delta^{13}C_{DIC}$ from the surface to mid-depth of

527   the Atlantic Ocean during periods of AMOC slowdown, although this decrease is more expres-

528   sive at intermediate and mid-depths of the tropical and North Atlantic (Menviel et al., 2018;

529   Schmittner and Lund, 2015). These simulations agree with $\delta^{13}C$ records of benthic foraminif-

530   era (e.g., Campos et al., 2020; Voigt et al., 2017; Oppo et al., 2015). Therefore, we suggest

531   that the $\delta^{13}C$ depletion observed at intermediate depth of the western tropical South Atlantic

532   (e.g., site GL-1180) was likely caused by the reduction of the North Atlantic overturning and

533   accumulation of isotopically light carbon at intermediate and mid-depths. Indeed, over the last

534   deglaciation, our benthic $\delta^{13}C$ record (Fig. 5c) presents the same "W-like" shape observed in

535   benthic $\delta^{13}C$ record of core M125-95-3 (Fig. 5d), collected from the mid-depth of the tropical

536   South Atlantic (Fig. 1) (Campos et al., 2020). The early $\delta^{13}C$ decrease in the GL-1180 benthic

537   record relative to other benthic records shown in Fig. 5 may result from the limited chronologic

24

538 control (6 radiocarbon ages) and the lower sampling resolution of GL-1180 over the early

539 deglaciation. No substantial chronological difference is found by calibrating the radiocarbon

540 ages of GL-1180 with the Marine20 calibration curve (Heaton et al. 2020) (Supporting Infor-

541 mation, Text S2). Given the location and resemblance of GL-1180 benthic record relative to

542 sediment cores M125-95-3 (Campos et al., 2020) and GS07-150-17/1GC-A (Freeman et al.,

543 2015) (Fig. 1 and Fig. 5), it is reasonable to assume that over the Termination I, the bottom of

544 the water column at these sites were influenced by a $\delta^{13}C$ signal of similar origin. Together,

545 these results support that the ^{13}C-depletion at intermediate depth of the tropical Atlantic is

546 mostly caused by the aged North Atlantic sourced waters. This interpretation can be applied

547 to $\delta^{13}C$ minimum events that occurred during previous glacial terminations, as seen in our

548 benthic record (Fig. 2a). Importantly, this hypothesis is dissociated from the "ocean tunnel"

549 and the ocean-atmosphere isotopic equilibration.

550 However, it has also been hypothesized that the thermodynamic equilibration could be

551 equally responsible for the $\delta^{13}C$ minimum observed at mid-depth of the Atlantic Ocean over

552 the last termination by affecting the formation region of the NADW (Lynch-Stieglitz et al.,

553 2019). However, a recent study showed that mid-depth benthic $\delta^{13}C$ minimum leads the plank-

554 tonic counterpart and atmospheric $\delta^{13}C$ by ~800 years (Lund et al., 2019). If the ocean-atmos-

555 phere isotopic equilibration was responsible for $\delta^{13}C$ minimum at mid-depth of the Atlantic

556 Ocean, one would expect the atmosphere to lead the ocean. Therefore, the lag of the atmos-

557 phere relative to the ocean implies that the ocean-atmosphere isotopic equilibration through

558 northern-sourced waters is unlikely to have been the main driver of the $\delta^{13}C$ minimum event

559 at intermediate and mid-depths of the Atlantic Ocean during Termination I.

560 In contrast to our reasoning of a northern-sourced $\delta^{13}C$ minimum at intermediate depth,

561 Poggemann et al. (2017) suggested an injection of nutrient-rich ^{13}C-depleted AAIW at inter-

562 mediate depth of the tropical North Atlantic during the last deglaciation (site M78/1-235-1; Fig.

563 1). This conclusion was based on benthic $\delta^{13}C$ and seawater-dissolved cadmium (Cd_w), a

564 proxy for phosphate concentration in seawater. However, as stressed above, the low $\delta^{13}C$

565 signal contradicts depth transects from the southern Brazilian margin (Lund et al., 2015; Tes-

566 sin and Lund, 2013; Oppo and Horowitz, 2000). While part of this Cd_w increase shown by

567 Poggemann et al. (2017) may result from the remineralization of organic matter and nutrient

568 accumulation due to the AMOC slowdown, another part must be decoupled from the $\delta^{13}C_{DIC}$

569 since records from the upper North Atlantic show that increases in Cd_w are not simultaneous

570 with $\delta^{13}C$ decreases (Lynch-Stieglitz et al., 2019). Indeed, a recent study showed that although

571 the $\delta^{13}C_{DIC}$ signal of upwelled deep waters is strongly affected by ocean-atmosphere isotopic

572 equilibration in the SO surface, nutrients are still transported northward through the "oceanic

573 tunnel" decoupled from $\delta^{13}C_{DIC}$ signal (Shao et al., 2021). Therefore, this result can help to

574 conciliate Cd_w and benthic $\delta^{13}C$ records from intermediate depth of the tropical Atlantic.

6. Conclusions

576   We present three high temporal resolution thermocline and intermediate depth (1037

577 m) foraminiferal $\delta^{13}C$ records from the western South Atlantic spanning the last 300 kyr. The

578 planktonic and benthic records show remarkable $\delta^{13}C$ minimum events during the last three

579 glacial terminations, as well as during the MIS 4/3 transition. Benthic $\delta^{13}C$ depth transects

580 from the south Brazilian margin, as well as intermediate depth $\delta^{13}C$ records from the Pacific

581 Ocean, contradict the long-held hypothesis of a northward advection of ^{13}C-depleted carbon

582 from the SO surface by SAMW and AAIW. Instead, we suggest that the $\delta^{13}C$ minima at the

583 thermocline and intermediate depths were governed by two distinct and independent mecha-

584 nisms. The good correspondence between predicted $\delta^{13}C_{DIC}$ and planktonic $\delta^{13}C$ from the

585 southern Brazilian margin indicates that the thermodynamic ocean-atmosphere isotopic equi-

586 libration strongly modulated the $\delta^{13}C_{DIC}$ signal in the western South Atlantic thermocline. This

587 mechanism can explain the global occurrence of $\delta^{13}C$ minimum events in the upper ocean

588 and agrees with recent numerical modeling. Indeed, the thermodynamic equilibration is a lead-

589 ing driver of the ^{13}C-depleted signal in the western South Atlantic thermocline during glacial

590 terminations and MIS 4/3 transition. However, in the domain of SAMW, changes in the biolog-

591 ical pump in the SAZ must also be considered. We propose that the origin of the $\delta^{13}C$ minimum

592 events at intermediate depths of the tropical Atlantic is related to the slow rate of NADW for-

593 mation during glacial terminations and the accumulation of remineralized carbon at mid and

594 intermediate depths of the tropical and North Atlantic. Importantly, the latter mechanism does

595 not evoke the deep ocean and upwelling in the SO as a source of ^{13}C-depleted carbon to

596 intermediate depths of the Atlantic Ocean.

Data availability

598   All data presented in the manuscript are available at [LINK]

References

618 Abernathey, R.P., Cerovecki, I., Holland, P.R., Newsom, E., Mazloff, M., Talley, L.D., (2016).

619 Water-mass transformation by sea ice in the upper branch of the Southern Ocean overturning.

620 Nat. Geosci. 9, 596–601. https://doi.org/10.1038/ngeo2749

621 Anderson, R.F., Ali, S., Bradtmiller, L.I., Nielsen, S.H.H., Fleisher, M.Q., Anderson, B.E.,

622 Burckle, L.H., (2009). Wind-Driven Upwelling in the Southern Ocean and the Deglacial Rise

623 in Atmospheric CO^2. Science, 323, 1443–1448. https://doi.org/1126/science.1167441

624 Arz, H. W., Pätzold, J., Wefer, G. (1999). The deglacial history of the western tropical Atlantic

625 as inferred from high resolution stable isotope records off northeastern Brazil, Earth Planet.

626 Sci. Lett., 167, 105–117, doi:10.1016/S0012-821X(99)00025-4.

627 Ballalai, J.M., Santos, T.P., Lessa, D.O., Venancio, I.M., Chiessi, C.M., Johnstone, H.J.H.,

628 Kuhnert, H., Claudio, M.R., Toledo, F., Costa, K.B., Albuquerque, A.L.S., (2019). Tracking

629 spread of the Agulhas leakage into the western South Atlantic and its northward transmission

630 during the last interglacial. Paleoceanogr. Paleoclimatol., 34(11), 1744-

631 1760. https://doi.org/10.1029/2019PA003653;

632 Barker, S., Diz, P., (2014). Timing of the descent into the last Ice Age determined by the bipolar

633 seesaw. Paleoceanography, 29, 489–507. https://doi.org/10.1002/2014PA002623

634 Barker, S., Diz, P., Vautravers, M.J., Pike, J., Knorr, G., Hall, I.R., Broecker, W.S., (2009).

635 Interhemispheric Atlantic seesaw response during the last deglaciation. Nature, 457, 1097–

636 1102. https://doi.org/10.1038/nature07770

637 Basak, C., Fröllje, H., Lamy, F., Gersonde, R., Benz, V., Anderson, R.F., Molina-Kescher, M.,

638 Pahnke, K., 2018. Breakup of last glacial deep stratification in the South Pacific. Science, 359,

639 900–904. https://doi.org/10.1126/science.aao2473

640 Bemis, B.E., Spero, H.J., Lea, D.W., Bijma, J., (2000). Temperature influence on the carbon

641 isotopic composition of *Globigerina bulloides* and *Orbulina universa* (planktonic foraminifera).

642 Mar. Micropaleontol., 38, 213–228. https://doi.org/10.1016/S0377-8398(00)00006-2

643 Bereiter, B., Lüthi, D., Siegrist, M., Schüpbach, S., Stocker, T.F., Fischer, H., (2012). Mode

644 change of millennial CO_2 variability during the last glacial cycle associated with a bipolar ma-

645 rine carbon seesaw. Proc. Natl. Acad. Sci. U. S. A., 109, 9755–9760.

646 https://doi.org/10.1073/pnas.1204069109

647 Birch, H., Coxall, H.K., Pearson, P.N., Kroon, D., O'Regan, M., (2013). Planktonic

648 foraminifera stable isotopes and water column structure: disentangling ecological signals. Mar.

649 Micropaleontol., 101, 127–145. https://doi.org/10.1016/j.marmicro.2013.02.002;

650 Blaauw, M. (2010). Methods and code for "classical" age-modelling of radiocarbon sequences.

651 Quat. Geochronol., 5(5), 512–518. http://doi.org/10.1016/j.quageo.2010.01.002

652 Blaauw, M., Christen, J. A. (2011). Flexible paleoclimate age-depth models using an auto-

653 regressive gamma process. Bayesian Anal., 6(3), 457–474. https://doi.org/10.1214/11-

654 BA618;

655 Bostock, H.C., Opdyke, B.N., Gagan, M.K. and Fifield, L.K., (2004). Carbon isotope evidence

656 for changes in Antarctic Intermediate Water circulation and ocean ventilation in the southwest

657 Pacific during the last deglaciation. Paleoceanography, 19(4).

658 https://doi.org/10.1029/2004PA001047

659 Broecker, W.S., Maier-Reimer, E., (1992). The influence of air and sea exchange on the

660 carbon isotope distribution in the sea. Glob. Biogeochem. Cycles 6, 315–320.

661 https://doi.org/10.1029/92GB01672

662 Burke, A., Robinson, L.F., (2012). The southern ocean's role in carbon exchange during the

663 last deglaciation. Science, 335, 557–561. https://doi.org/10.1126/science.1208163

664 Campos, M.C., Chiessi, C.M., Venancio, I.M., Pinho, T.M.L., Crivellari, S., Kuhnert, H.,

665 Schmiedl, G., Díaz, R.A., Albuquerque, A.L.S., Portilho-Ramos, R.C., Bahr, A., Mulitza, S.,

666 (2020). Constraining Millennial-Scale Changes in Northern Component Water Ventilation in

667 the Western Tropical South Atlantic, Paleoceanogr. Paleoclimatol..

668 https://doi.org/10.1029/2020PA003876

669 Chen, T., Robinson, L.F., Burke, A., Claxton, L., Hain, M.P., Li, T., Rae, J.W., Stewart, J.,

670 Knowles, T.D., Fornari, D.J. and Harpp, K.S., 2020. Persistently well-ventilated intermediate-

671 depth ocean through the last deglaciation. Nat. Geosci., 13(11), pp.733-738.

672 https://doi.org/10.1038/s41561-020-0638-6

673 Chiessi, C.M., Ulrich, S., Mulitza, S., Pätzold, J., Wefer, G. (2007). Signature of the

674 Brazil-Malvinas Confluence (Argentine Basin) in the isotopic composition of

675 planktonic foraminifera from surface sediments. Mar. Micropaleontol., 64, 52–66.

676 https://doi.org/10.1016/j.marmicro.2007.02.002;

677 Cléroux, C., Cortijo, E., Duplessy, J.C., Zahn, R. (2007). Deep-dwelling foraminifera as

678 thermocline temperature recorders. Geochem. Geophys. Geosys., 8(4).

679 https://doi.org/10.1029/2006GC001474;

680 Cléroux, C., deMenocal, P. and Guilderson, T., 2011. Deglacial radiocarbon history of tropical

681 Atlantic thermocline waters: absence of CO_2 reservoir purging signal. Quat. Sci. Rev., 30(15-

682 16), pp.1875-1882. https://doi.org/10.1016/j.quascirev.2011.04.015

683 Cléroux, C., Demenocal, P., Arbuszewski, J., Linsley, B., (2013). Reconstructing the upper

684 water column thermal structure in the Atlantic Ocean. Paleoceanography 28, 503–516.

685 https://doi.org/10.1002/palo.20050

686 Crivellari, S., Viana, P.J., Campos, M.C., Kuhnert, H., Barros, A., Cruz, F.W., Chiessi, C.M.,

687 (2021). Development and characterization of a new in-house reference material for stable car-

688 bon and oxygen isotopes analyses. Journal of Analytical Atomic Spectrometry.

689 DOI 10.1039/D1JA00030F

690 Curry, W.B., Oppo, D.W., (2005). Glacial water mass geometry and the distribution of $\delta^{13}C$ of

691 ΣCO_2 in the western Atlantic Ocean. Paleoceanography 20, 1–12.

692 https://doi.org/10.1029/2004PA001021

693 Du, J., Haley, B.A., Mix, A.C., Walczak, M.H., Praetorius, S.K., (2018). Flushing of the deep

694 Pacific Ocean and the deglacial rise of atmospheric CO_2 concentrations. Nat. Geosci. 11, 749–

695 755. https://doi.org/10.1038/s41561-018-0205-6

696 Eggleston, S., Schmitt, J., Bereiter, B., Schneider, R., Fischer, H., (2016). Evolution of the

697 stable carbon isotope composition of atmospheric CO_2 over the last glacial cycle. Paleocean-

698 ography 31, 434–452. https://doi.org/10.1002/2015PA002874

699 Eide, M., Olsen, A., Ninnemann, U.S., Johannessen, T., (2017). A global ocean climatology

700 of preindustrial and modern ocean $\delta^{13}C$. Glob. Biogeochem. Cycles 31, 515–534.

701 https://doi.org/10.1002/2016GB005473

702 Elderfield, H., Vautravers, M., Cooper, M., (2002). The relationship between shell size and

703 Mg/Ca, Sr/Ca, $\delta^{18}O$, and $\delta^{13}C$ of species of planktonic foraminifera. Geochem. Geophys.

704 Geosys., 3, 1–13. https://doi.org/10.1029/2001gc000194

705 Emery, W., Meincke, J., (1986). Global water masses: summary and review. Oceanol. Acta,

706 9, 383–391.

707 England, M.H., Godfrey, J.S., Hirst, A.C., Tomczak, M., 1993. The mechanism for Antarctic

708 Intermediate Water renewal in a world ocean model. J. Phys. Oceanogr., *23*(7), 1553-1560.

709 https://doi.org/10.1175/1520 0485(1993)023<1553:TMFAIW>2.0.CO;2

710 Farmer, E.C., Kaplan, A., de Menocal, P.B., Lynch-Stieglitz, J., (2007). Corroborating ecolog-

711 ical depth preferences of planktonic foraminifera in the tropical Atlantic with the stable oxygen

712 isotope ratios of core top specimens. Paleoceanography 22, 1–14.

713 https://doi.org/10.1029/2006PA001361

714 Feldmeijer, W., Metcalfe, B., Brummer, G., Ganssen, G. (2014). Reconstructing the depth of

715 the permanent thermocline through the morphology and geochemistry of the deep dwelling

716 planktonic foraminifer *Globorotalia truncatulinoides*. Paleoceanography, 30, 1–22.

717 https://doi.org/10.1002/2014PA002687

718 Freeman, E., Skinner, L.C., Tisserand, A., Dokken, T., Timmermann, A., Menviel, L., Friedrich,

719 T., (2015). An Atlantic-Pacific ventilation seesaw across the last deglaciation. Earth Planet.

720 Sci. Lett. 424, 237–244. https://doi.org/10.1016/j.epsl.2015.05.032

721 Friedrich, O., Schiebel, R., Wilson, P.A., Weldeab, S., Beer, C.J., Cooper, M.J., Fiebig, J.,

722 (2012). Influence of test size, water depth, and ecology on Mg/Ca, Sr/Ca, $\delta^{18}O$ and $\delta^{13}C$ in

723 nine modern species of planktic foraminifers. Earth Planet. Sci. Lett. 319–320, 133–145.

724 https://doi.org/10.1016/j.epsl.2011.12.002

725 Gebbie, G. (2014). How much did glacial North Atlantic water shoal? Paleoceanography, 29,

726 190‑209. https://doi.org/10.1002/2013PA002557

727 Gersonde, R. and Zielinski, U., (2000). The reconstruction of late Quaternary Antarctic sea-

728 ice distribution—the use of diatoms as a proxy for sea-ice. Palaeogeogr. Palaeoclimatol. Pa-

729 laeoecol., 162(3-4), 263-286. https://doi.org/10.1016/S0031-0182(00)00131-0

730 Gray, W.R., Evans, D., (2019). Nonthermal Influences on Mg/ca in Planktonic

731 Foraminifera: a Review of Culture Studies and Application to the last Glacial

732 Maximum. Paleoceanogr. Paleoclimatol. 34, 306‑315. https://doi.org/10.1029/

733 2018PA003517.

734   Gordon, A.L., (1986). Interocean exchange of thermocline water. Journal of Geophysical Re-

735   search, 91, 5037-5046. https://doi.org/10.1029/JC091iC04p05037

736   Govin, A., Capron, E., Tzedakis, P.C., Verheyden, S., Ghaleb, B., Hillaire-Marcel, C., St-Onge,

737   G., Stoner, J.S., Bassinot, F., Bazin, L., Blunier, T., (2015). Sequence of events from the onset

738   to the demise of the Last Interglacial: Evaluating strengths and limitations of chronologies used

739   in climatic archives. Quat. Sci. Rev., 129, 1–36. http://doi.org/10.1016/j.quasci-

740   rev.2015.09.018;

741   Govin, A., Chiessi, C.M., Zabel, M., Sawakuchi, A.O., Heslop, D., Hörner, T.,

742   Zhang, Y., Mulitza, S., (2014). Terrigenous input off northern South America driven by

743   changes in Amazonian climate and the North Brazil Current retroflection during the last 250

744   ka. Clim. Past 10, 843–862. http://dx.doi.org/ 10.5194/cp-10-843-2014.

745   Groeneveld, J., Chiessi, C.M., (2011). Mg/Ca of *Globorotalia inflata* as a recorder of perma-

746   nent thermocline temperatures in the South Atlantic. Paleoceanography 26, 1–12.

747   https://doi.org/10.1029/2010PA001940

748   Heaton, T.J., Köhler, P., Butzin, M., Bard, E., Reimer, R.W., Austin, W.E., Ramsey, C.B.,

749   Grootes, P.M., Hughen, K.A., Kromer, B. and Reimer, P.J., 2020. Marine20—the marine radi-

750   ocarbon age calibration curve (0–55,000 cal BP). *Radiocarbon*, *62*(4), pp.779-820.

751   https://doi.org/10.1017/RDC.2020.68

752   Hertzberg, J.E., Lund, D.C., Schmittner, A., Skrivanek, A.L., (2016). Evidence for a biological

753   pump driver of atmospheric CO_2 rise during Heinrich Stadial 1. Geophys. Res. Lett. 43,

754   12,242-12,251. https://doi.org/10.1002/2016GL070723

755   Hodell, D.A., Venz, K.A., Charles, C.D., Ninnemann, U.S., (2003). Pleistocene vertical carbon

756   isotope and carbonate gradients in the South Atlantic sector of the Southern Ocean, Geo-

757   chem. Geophys. Geosys., 4, 1–19. https://doi.org/10.1029/2002GC000367

758 Howe, J.N.W., Piotrowski, A.M., Noble, T.L., Mulitza, S., Chiessi, C.M., Bayon, G., (2016a).

759 North Atlantic Deep Water Production during the Last Glacial Maximum. Nat. Commun. 7, 1–

760 8. https://doi.org/10.1038/ncomms11765

761 Hu, R., Bostock, H.C., Greaves, M., Piotrowski, A.M., McCave, I.N., (2020). Coupled evolution

762 of stable carbon isotopes between the Southern Ocean and the atmosphere over the last 260

763 ka. Earth Planet. Sci. Lett. 538, 116215. https://doi.org/10.1016/j.epsl.2020.116215

764 Jaccard, S.L., Hayes, C.T., Martinez-Garcia, A., Hodell, D.A., Anderson, R.F., Sigman, D.M.

765 and Haug, G.H., 2013. Two modes of change in Southern Ocean productivity over the past

766 million years. Science, 339(6126), pp.1419-1423. https://doi.org/10.1126/science.1227545

767 Kohfeld, K.E.,Chase, Z., (2017). Temporal evolution of mechanisms controlling ocean carbon

768 uptake during the last glacial cycle. Earth Planet. Sci. Lett., 472, 206-215.

769 https://doi.org/10.1016/j.epsl.2017.05.015

770 Lacerra, M., Lund, D., Yu, J., Schmittner, A., (2017). Carbon storage in the mid-depth Atlantic

771 during millennial-scale climate events. Paleoceanography 32, 780–795.

772 https://doi.org/10.1002/2016PA003081

773 LeGrande, A.N., Lynch-Stieglitz, J., Farmer, E.C., (2004). Oxygen isotopic composition of *Glo-*

774 *borotalia truncatulinoides* as a proxy for intermediate depth density. Paleoceanography, 19,

775 PA4025. https://doi.org/10,1029/2004PA001045

776 Liu, Z. and Yang, H., (2003). Extratropical control of tropical climate, the

777 atmospheric bridge and oceanic tunnel, Geophys. Res. Lett, 30,

778 1230, doi:10.1029/2002GL016492

779 Lisiecki, L. E., Raymo, M. E. (2005). A Pliocene-Pleistocene stack of 57 globally distributed

780 benthic $\delta^{18}O$ records. Paleoceanography, *20*(1), 1–17. https://doi.org/10.1029/2004PA001071

781   Lund, D., Hertzberg, J., Lacerra, M., (2019). Carbon isotope minima in the South Atlantic dur-

782   ing the last deglaciation: Evaluating the influence of air-sea gas exchange. Environ. Res. Lett.

783   14. https://doi.org/10.1088/1748-9326/ab126f

784   Lund, D.C., Tessin, A.C., Hoffman, J.L., Schmittner, A., (2015). Southwest Atlantic water mass

785   evolution during the last deglaciation. Paleoceanography 30, 477–494.

786   https://doi.org/10.1002/2014PA002657

787   Lynch-Stieglitz, J., R.G. Fairbanks (1994). A conservative tracer for glacial ocean circulation

788   from carbon isotope and paleo-nutrient measurements in benthic foraminifera. Nature, 369,

789   308-310. https://doi.org/10.1038/369308a0

790   Lynch-Stieglitz, J., Stocker, T.F., Broecker, W.S., Fairbanks, R.G., (1995). The influence of

791   air–sea exchange on the isotopic composition of oceanic carbon – observations

792   and modeling. Glob. Biogeochem. Cycles 9, 653–665. https://doi.org/10.1029/95GB02574

793   Lynch-Stieglitz, J., Valley, S.G., Schmidt, M.W., (2019). Temperature-dependent ocean–at-

794   mosphere equilibration of carbon isotopes in surface and intermediate waters over the degla-

795   ciation. Earth Planet. Sci. Lett. 506, 466–475. https://doi.org/10.1016/j.epsl.2018.11.024

796   Marshall, J., Speer, K., (2012). Closure of the meridional overturning circulation through

797   Southern Ocean upwelling. Nat. Geosci. 5, 171–180. https://doi.org/10.1038/ngeo1391

798   Martínez-Botí, M.A., Marino, G., Foster, G.L., Ziveri, P., Henehan, M.J., Rae, J.W.B., Mortyn,

799   P.G., Vance, D., (2015). Boron isotope evidence for oceanic carbon dioxide leakage during

800   the last deglaciation. Nature 518, 219–222. https://doi.org/10.1038/nature14155

801   Martínez-García, A., Sigman, D.M., Ren, H., Anderson, R.F., Straub, M., Hodell, D.A., Jac-

802   card, S.L., Eglinton, T.I. and Haug, G.H., 2014. Iron fertilization of the Subantarctic Ocean

803   during the last ice age. Science, 343(6177), pp.1347-1350. https://doi.org/10.1126/sci-

804   ence.1246848

805   Menviel, L., Spencer, P., Yu, J., Chamberlain, M.A., Matear, R.J., Meissner, K.J., England,

806   M.H., (2018). Southern Hemisphere westerlies as a driver of the early deglacial atmospheric

807   CO_2 rise. Nat. Commun. 1–12. https://doi.org/10.1038/s41467-018-04876-4

808   Mulitza, S., Arz, H., Kemle-von Mucke, S., Moos, C., Niebler, H.S., Pätzold, J., Segl, M. (1999).

809   The South Atlantic carbon isotope record of planktonic foraminifera. In *Use of Proxies in*

810   *Paleocanography: Examples from the South Atlantic* (ed. Fischer, G. and Wefer, G.) (Berlin:

811   Springer), 427–445.

812   Mulitza, S., Dürkoop, A., Hale, W., Wefer, G., Niebler, H. S. (1997). Planktonic foraminifera as

813   recorders   of   past   surface-water   stratification.   Geology,   25(4),   335–

814   338. https://doi.org/10.1130/0091-7613(1997)025<0335:PFAROP>2.3.CO;2;

815   Mulitza, S., Rühlemann, C., Bickert, T., Hale, W., Pätzold, J., Wefer, G., (1998). Late Quater-

816   nary $\delta^{13}C$ gradients and carbonate accumulation in the western equatorial Atlantic. Earth

817   Planet. Sci. Lett. 155, 237–249. https://doi.org/10.1016/s0012-821x(98)00012-0

818   Mulitza, S., Chiessi, C.M., Schefuß, E., Lippold, J., Wichmann, D., Antz, B., Mackensen, A.,

819   Paul, A., Prange, M., Rehfeld, K. and Werner, M., (2017). Synchronous and proportional de-

820   glacial changes in Atlantic meridional overturning and northeast Brazilian precipita-

821   tion. Paleoceanography, 32(6), pp.622-633. https://doi.org/10.1002/2017PA003084

822   Nascimento, R. A., Venancio, I. M., Chiessi, C. M., Ballalai, J. M., Kuhnert, H., Johnstone, H.,

823   Santos, T. P., Prange, M., Govin, A., Crivellari, S., Mulitza, S., Albuquerque, A. L. S., (2021).

824   Tropical Atlantic stratification response to late Quaternary precessional forcing. Earth Planet.

825   Sci. Lett., 568, 117030, https://doi.org/10.1016/j.epsl.2021.117030

826   NGRIP community members, 2004. High-resolution record of Northern Hemisphere

827   climate   extending   into   the   last   interglacial   period.   Nature   431,   147-151.

828   https://doi.org/10.1038/nature02805

829   Ninnemann, U.S., Charles, C.D., (1997). Regional differences in Quaternary Subantarctic nu-

830   trient cycling: Link to intermediate and deep-water ventilation. Paleoceanography 12, 560–

831   567. https://doi.org/10.1029/97PA01032

832   Oppo, D.W., Curry, W.B., McManus, J.F., (2015). What do benthic δ^{13}C and δ^{18}O data tell us

833   about Atlantic circulation during Heinrich Stadial 1? Paleoceanography 30, 353–368.

834   https://doi.org/10.1002/2014PA002667

835   Oppo, D.W., Gebbie, G., Huang, K.F., Curry, W.B., Marchitto, T.M. and Pietro, K.R., 2018.

836   Data constraints on Glacial Atlantic water mass geometry and properties. Paleoceanogr. Pa-

837   leoclimatol., 33(9), pp.1013-1034. https://doi.org/10.1029/2018PA003408

838   Oppo, D.W., Horowitz, M., 2000. Glacial deep-water geometry: South Atlantic benthic forami-

839   niferal   Cd/Ca   and   δ13C   evidence. Paleoceanography, 15(2),   pp.147-

840   160. https://doi.org/10.1029/1999PA000436

841   Orsi, A.H., Whitworth III, T. and Nowlin Jr, W.D., (1995). On the meridional extent and fronts

842   of the Antarctic Circumpolar Current. Deep Sea Res. Part I Oceanogr. Res. Pap., 42(5),

843   pp.641-673. https://doi.org/10.1016/0967-0637(95)00021-W

844   Pahnke, K., Zahn, R., (2005). Southern Hemisphere water mass conversion linked with North

845   Atlantic climate variability. Science, 307(5716), 1741-1746. http://doi.org/10.1126/sci-

846   ence.1102163

847   Pellichero, V., Sallée, J.B., Chapman, C.C., Downes, S.M., (2018). The Southern Ocean me-

848   ridional overturning in the sea-ice sector is driven by freshwater fluxes. Nat. Commun. 9.

849   https://doi.org/10.1038/s41467-018-04101-2

850   Pena, L.D., Goldstein, S.L., Hemming, S.R., Jones, K.M., Calvo, E., Pelejero, C., Cacho, I.,

851   (2013). Rapid changes in meridional advection of Southern Ocean intermediate waters to the

852 tropical Pacific during the last 30kyr. Earth Planet. Sci. Lett. 368, 20–32.
853 https://doi.org/10.1016/j.epsl.2013.02.028

854 Pereira, L.S., Arz, H.W., Pätzold, J. and Portilho-Ramos, R.C., (2018). Productivity evolution
855 in the South Brazilian Bight during the last 40,000 years. Paleoceanogr. Paleoclima-
856 tol., *33*(12), 1339-1356. https://doi.org/10.1029/2018PA003406

857 Peterson, R.G., Stramma, L., (1991). Upper-level circulation in the South Atlantic Ocean 26,
858 1–73. https://doi.org/10.1016/0079-6611(91)90006-8

859 Poggemann, D., Hathorne, E.C., Nürnberg, D., Frank, M., Bruhn, I., Reißig, S., Bahr, A.,
860 (2017). Rapid deglacial injection of nutrients into the tropical Atlantic via Antarctic Intermediate
861 Water. Earth Planet. Sci. Lett. 463, 118–126. https://doi.org/10.1016/j.epsl.2017.01.030

862 Poole, R., Tomczak, M. (1999). Optimal multiparameter analysis of the water mass structure
863 in the Atlantic Ocean thermocline. Deep-Sea Res. I: Oceanographic Research Papers, 46 (11),
864 1895-1921. https://doi.org/10.1016/S0967-0637(99)00025-4;

865 Ravelo, A. C., Hillaire-Marcel, C. (2007). The use of oxygen and carbon isotopes of foraminif-
866 era in paleoceanography. Developments in marine geology, 1, 735-764.

867 Regenberg, M., Steph, S., Nürnberg, D., Tiedemann, R., Garbe-Schönberg, D. (2009). Cali-
868 brating Mg/Ca ratios of multiple planktonic foraminiferal species with $\delta^{18}O$-calcification tem-
869 peratures: Paleothermometry for the upper water column. Earth Planet. Sci. Lett., 278(3–4),
870 324–336. https://doi.org/10.1016/j.epsl.2008.12.019;

871 Reimer, P.J., Bard, E., Bayliss, A., Beck, J.W., Blackwell, P.G., Ramsey, C.B., Buck, C.E.,
872 Cheng, H., Edwards, R.L., Friedrich, M., Grootes, P.M., (2013). IntCal13 and Marine13 radio-
873 carbon age calibration curves 0–50,000 years cal BP. Radiocarbon, 55(04), 1869–1887.
874 https://doi.org/10.2458/azu_js_rc.55.16947;

875 Rickaby, R.E.M., Elderfield, H., 2005. Evidence from the high-latitude North Atlantic for varia-

876 tions in Antarctic Intermediate water flow during the last deglaciation. Geochem. Geophys.

877 Geosys., 6(5). https://doi.org/10.1029/2004GC000858

878 Romanek, C.S., Grossman, E.L., Morse, J.W., (1992). Carbon isotopic fractionation in syn-

879 thetic aragonite and calcite: effects of temperature and precipitation rate. Geochimica et cos-

880 mochimica acta, 56(1), 419-430. https://doi.org/10.1016/0016-7037(92)90142-6

881 Santos, T.P., Ballalai, J.M., Franco, D.R., Oliveira, R.R., Lessa, D.O., Venancio, I.M., Chiessi,

882 C.M., Kuhnert, H., Johnstone, H., Albuquerque, A.L.S. (2020). Asymmetric response of the

883 subtropical western South Atlantic thermocline to the Dansgaard-Oeschger events of Marine

884 Isotope Stages 5 and 3. Quat. Sci. Rev., 236. https://doi.org/10.1016/j.quascirev.2020.106307

885 Santos, T.P., Lessa, D.O., Venancio, I.M., Chiessi, C.M., Mulitza, S., Kuhnert, H., Govin, A.,

886 Machado, T., Costa, K.B., Toledo, F., Dias, B.B., Albuquerque, A.L.S. (2017). Prolonged

887 warming of the Brazil Current precedes deglaciations. Earth Planet. Sci. Lett., 463, 1-12.

888 https://doi.org/10.1016/j.epsl.2017.01.014.

889 Schaefer, J.M., Putnam, A.E., Denton, G.H., Kaplan, M.R., Birkel, S., Doughty, A.M., Kelley,

890 S., Barrell, D.J.A., Finkel, R.C., Winckler, G., Anderson, R.F., Ninneman, U.S., Barker, S.,

891 Schwartz, R., Andersen, B.G., Schluechter, C., (2015). The Southern Glacial Maximum 65,000

892 years ago and its Unfinished Termination. Quat. Sci. Rev., 114, 52–60.

893 https://doi.org/10.1016/j.quascirev.2015.02.009

894 Schlitzer, R. (2017). Ocean Data View, odv.awi.de;

895 Schmitt, J., Schmitt, J., Schneider, R., Elsig, J., Leuenberger, D., Lourantou, A., Chappellaz,

896 J., Köhler, P., Joos, F., Stocker, T.F., Leuenberger, M., Fischer, H., (2012). Carbon isotope

897 constraints on the deglacial CO_2 rise from ice cores. Science, 336(6082), 711-714.

898 https://doi.org/10.1126/science.1217161

899   Schmittner, A., Lund, D.C., (2015). Early deglacial Atlantic overturning decline and its role in

900   atmospheric CO^2 rise inferred from carbon isotopes (δ^{13}C). Clim. Past 11, 135–152.

901   https://doi.org/10.5194/cp-11-135-2015

902   Schneider, R., Schmitt, J., Köhler, P., Joos, F., Fischer, H., (2013). A reconstruction of atmos-

903   pheric carbon dioxide and its stable carbon isotopic composition from the penultimate glacial

904   maximum   to   the   last   glacial   inception,   Clim.   Past,   9(6),   2507–2523,

905   doi:10.5194/cp-9-2507-2013.

906   Shao, J., Stott, L., Menviel, L., Ridgwell, A., Ödalen, M., Mohtadi, M., (2021). The Atmospheric

907   Bridge Communicated the δ^{13}C Decline during the Last Deglaciation to the Global Upper

908   Ocean. Clim. Past Discuss. 1–28. https://doi.org/10.5194/cp-2020-95

909   Skinner, L.C., Fallon, S., Waelbroeck, C., Michel, E., Barker, S., (2010). Ventilation of the

910   Deep Southern and Deglacial CO_2 Rise. Science 328, 1147–1151. https://doi.org/10.1126/sci-

911   ence.1183627

912   Sortor, R.N., Lund, D.C., (2011). No evidence for a deglacial intermediate water Δ^{14}C anomaly

913   in   the   SW   Atlantic.   Earth   Planet.   Sci.   Lett.   310,   65–72.

914   https://doi.org/10.1016/j.epsl.2011.07.017

915   Spero, H.J., Bijma, J., Lea, D.W., Bernis, B.E., (1997). Effect of seawater carbonate concen-

916   tration   on   foraminiferal   carbon   and   oxygen   isotopes.   Nature   390,   497–500.

917   https://doi.org/10.1038/37333

918   Spero, H.J., Deniro, M., (1987). The Influence of Symbiont Photosynthesis on the δ^{18}O and

919   δ^{13}C Values of Planktonic Foraminiferal Shell Calcite, Symbiosis, 4, 213–228.

920   Spero, H.J., Lea, D.W., (2002). The Cause of Carbon Isotope Minimum Events on Glacial

921   Terminations, Science, 296, 522–525. https://doi.org/10.1126/science.1069401

922   Sprintall, J., Tomczak, M., (1993). On the formation of Central Water and thermocline ventila-

923   tion in the southern hemisphere. Deep. Res. I. 40, 827-848. https://doi.org/10.1016/0967-

924   0637(93)90074-D;

925   Steph, S., Regenberg, M., Tiedemann, R., Mulitza, S., Nürnberg, D. (2009). Stable isotopes

926   of planktonic foraminifera from tropical Atlantic/Caribbean core-tops: Implications for recon-

927   structing   upper   ocean   stratification.   Mar.   Micropaleontol.,   *71*(1–2),   1–19.

928   https://doi.org/10.1016/j.marmicro.2008.12.004;

929   Stramma, L., England, M. (1999). On the water masses and mean circulation of the South

930   Atlantic   Ocean.   J.   Geophys.   Res.,   v.   104,   p.   20.863-20.883.

931   https://doi.org/10.1029/1999JC900139;

932   Talley, L.D., (1996). Antarctic Intermediate Water in the South Atlantic. In *The South Atlantic:*

933   *present and past circulation* (Ed. Wefer, G., Berger, W.H., Siedler, G., Webb, D.J.,) 219–238.

934   https://doi.org/10.1007/978-3-642-80353-6_11

935   Talley, L.D., (2013). Closure of the Global Overturning Circulation Through the Indian, Pacific,

936   and   Southern   Oceans: Schematics   and   Transports.   Oceanography   26,   80–97.

937   https://doi.org/10.5670/oceanog.2013.07

938   Tapia, R., Nürnberg, D., Ho, S.L., Lamy, F., Ullermann, J., Gersonde, R., Tiedemann, R.,

939   (2019). Glacial differences of Southern Ocean Intermediate Waters in the Central South Pa-

940   cific. Quat. Sci. Rev. 208, 105–117. https://doi.org/10.1016/j.quascirev.2019.01.016

941   Tessin, A.C., Lund, D.C., (2013). Isotopically depleted carbon in the mid-depth South Atlantic

942   during   the   last   deglaciation.   Paleoceanography   28,   296–306.

943   https://doi.org/10.1002/palo.20026

944   Toggweiler, J.R., Russell, J.L., Carson, S.R., (2006). Midlatitude westerlies, atmospheric CO_2,

945   and climate change during the ice ages, Paleoceanography 21, 1–15.

946   https://doi.org/10.1029/2005PA001154

947   Toggweiler, J.R., Samuels, B., (1995). Effect of Drake Passage on the global thermohaline.

948   Deep. Res. I 42, 477–500. https://doi.org/10.1016/0967-0637(95)00012-U

949   Tomczak, M., Godfrey, J.S., (1994). Regional Oceanography, 1st ed, Regional Oceanogra-

950   phy. Elsevier.

951   Ujiié, Y., de Garidel-Thoron, T., Wantanabe, S., Wiebe, P., de Vargas, C. (2010). Coiling di-

952   morphism within a genetic type of the planktonic foraminifer *Globorotalia truncatulinoides*. Mar.

953   Micropaleontol., 77(3-4), 145–153. https://doi.org/10.1016/j.marmicro.2010.09.001

954   Venancio, I.M., Mulitza, S., Govin, A., Santos, T.P., Lessa, D.O., Albuquerque, A.L.S., Chiessi,

955   C.M., Tiedemann, R., Vahlenkamp, M., Bickert, T., Schulz, M., (2018). Millennial- to orbital-

956   scale responses of Western Equatorial Atlantic thermocline depth to changes in the trade wind

957   system since the last interglacial. Paleoceanogr. Paleoclimatol., *33*(12), 1490–1507.

958   https://doi.org/10.1029/2018PA003437;

959   Voigt, I., Cruz, A.P.S., Mulitza, S., Chiessi, C.M., Mackensen, A., Lippold, J., Antz, B., Zabel,

960   M., Zhang, Y., Barbosa, C.F., Tisserand, A.A., (2017). Variability in mid-depth ventilation of

961   the western Atlantic Ocean during the last deglaciation. Paleoceanography 32, 948–965.

962   https://doi.org/10.1002/2017PA003095

963   WAIS (West Antarctic Ice Sheet Project) members (2013). Onset of deglacial warming in West

964   Antarctica driven by local orbital forcing. Nature 500, 440–444. https://doi.org/10.1038/na-

965   ture12376

966   Wilke, I., Bickert, T., Peeters, F.J.C., (2006). The influence of seawater carbonate ion concen-

967   tration [CO_3^{2-}] on the stable carbon isotope composition of the planktic foraminifera species

968   *Globorotalia inflata*. Mar. Micropaleontol. 58, 243–258. https://doi.org/10.1016/j.marmi-

969   cro.2005.11.005

970   Wolff, E.W., Chappellaz, J., Blunier, T., Rasmussen, S.O., Svensson, A., (2010). Millennial-

971   scale variability during the last glacial: The ice core record. Quat. Sci. Rev., 29(21-22), 2828-

972   2838. https://doi.org/10.1016/j.quascirev.2009.10.013

973   Wolff, E.W., Fischer, H., Röthlisberger, R., (2009). Glacial terminations as southern warmings

974   without northern control. Nat. Geosci. 2, 206–209. https://doi.org/10.1038/ngeo442

975   Zhang, J., Quay, P.D., Wilbur, D.O., 1995. Carbon-isotope fractionation during gaswater ex-

976   change and dissolution of CO_2. Geochim. Cosmochim. Acta 59, 107–114.

977   https://doi.org/10.1016/0016-7037(95)91550-D

978   Zhang, Y., Chiessi, C.M., Mulitza, S., Sawakuchi, A.O., Häggi, C., Zabel, M., Portilho-Ramos,

979   R.C., Schefuß, E., Crivellari, S., Wefer, G., (2017). Different precipitation patterns across trop-

980   ical South America during Heinrich and Dansgaard-Oeschger stadials. Quat. Sci. Rev., *177*,

981   1-9. https://doi.org/10.1016/j.quascirev.2017.10.012

982   Ziegler, M., Diz, P., Hall, I.R., Zahn, R., (2013). Millennial-scale changes in atmospheric CO_2

983   levels linked to the Southern Ocean carbon isotope gradient and dust flux. Nat. Geosci. 6,

984   457–461. https://doi.org/10.1038/ngeo1782

985   Zweng, M. M., J. R. Reagan, D. Seidov, T. P. Boyer, R. A. Locarnini, H. E. Garcia, A. V.

986   Mishonov, O. K. Baranova, K. Weathers, C. R. Paver, and I. Smolyar, 2018. World Ocean

987   Atlas 2018, Volume 2: Salinity. A. Mishonov Technical Ed.; NOAA Atlas NESDIS 82, 50pp.

988

989